An Examination of the Arctic Environment and Arctic Cyclones During Periods of Low and High Forecast Skill of the Synoptic-Scale Flow

Kevin A. Biernat
Department of Atmospheric and Environmental Sciences
University at Albany, State University of New York

Ph.D. Dissertation Defense
Thursday 16 December 2021

Committee Members: Lance Bosart, Daniel Keyser, Steven Cavallo, Andrea Lang, and Ryan Torn

Research Supported by ONR Grant N00014-18-1-2200

Motivation

- The Arctic environment is rapidly changing in response to enhanced near-surface warming relative to the rest of the globe, referred to as Arctic amplification, and diminishing sea ice (e.g., Stroeve et al. 2007; Screen and Simmonds 2010).

- As the Arctic environment rapidly changes, human activities, including shipping, tourism, and military operations, are increasing in the Arctic (e.g., Hall and Saarinen 2010; Melia et al. 2016, 2017; U.S. Department of the Navy 2021).

- Accurate weather prediction over the Arctic is important given that these human activities can be impacted by weather conditions in the Arctic.

- There has been a dearth of research concerning Arctic environmental conditions associated with periods of low and high forecast skill of the synoptic-scale flow over the Arctic, aside from a recent study by Yamagami and Matsueda (2021).

Motivation

- Arctic cyclones (ACs) are extratropical cyclones that may originate within the Arctic or move into the Arctic from lower latitudes (e.g., Serreze 1995; Zhang et al. 2004; Serreze and Barrett 2008; Crawford and Serreze 2016).

- ACs occur most frequently during summer (e.g., Zhang et al. 2004; Serreze and Barrett 2008) and may play important roles in influencing Arctic environmental conditions and the forecast skill of the synoptic-scale flow over the Arctic (e.g., Yamagami and Matsueda 2021).

- ACs may be associated with strong surface winds and high waves (e.g., Zhang et al. 2013; Thomson and Rogers 2014), and may contribute to rapid sea ice loss and rapid sea ice movement (e.g., Asplin et al. 2012; Stern et al. 2020; Peng et al. 2021).

Motivation

- Previous studies that have examined features and processes influencing the evolution of ACs have primarily been conducted through case studies of selected ACs (e.g., Simmonds and Rudeva 2012; Tao et al. 2017a,b; Yamagami et al. 2017).

- There have been a limited number of studies that have examined features and processes influencing the forecast skill of ACs (e.g., Tao et al. 2017b; Yamagami et al. 2018a; Johnson and Wang 2021).

Objectives

1) Examine characteristics of the Arctic environment, and the frequency, characteristics, and forecast skill of ACs, during periods of low and high forecast skill of the synoptic-scale flow over the Arctic, hereafter referred to as low-skill periods and high-skill periods, respectively.

2) Examine features and processes influencing the evolution of strong low-skill ACs during low-skill periods and strong high-skill ACs during low-skill periods.

3) Examine features and processes influencing the forecast skill of a selected strong low-skill AC during a low-skill period.

Literature review: Forecast skill over the Arctic

- Yamagami and Matsueda (2021) identify forecast busts over the Arctic based on day-6 forecasts of 500-hPa geopotential height over the Arctic for five different ensemble prediction systems (EPSs) during 2008–2019.

- They find that one of the most frequent Arctic weather patterns associated with forecast busts during summer at forecast initialization is the “Arctic Cyclone” pattern.

Literature review: Forecast skill over the Arctic

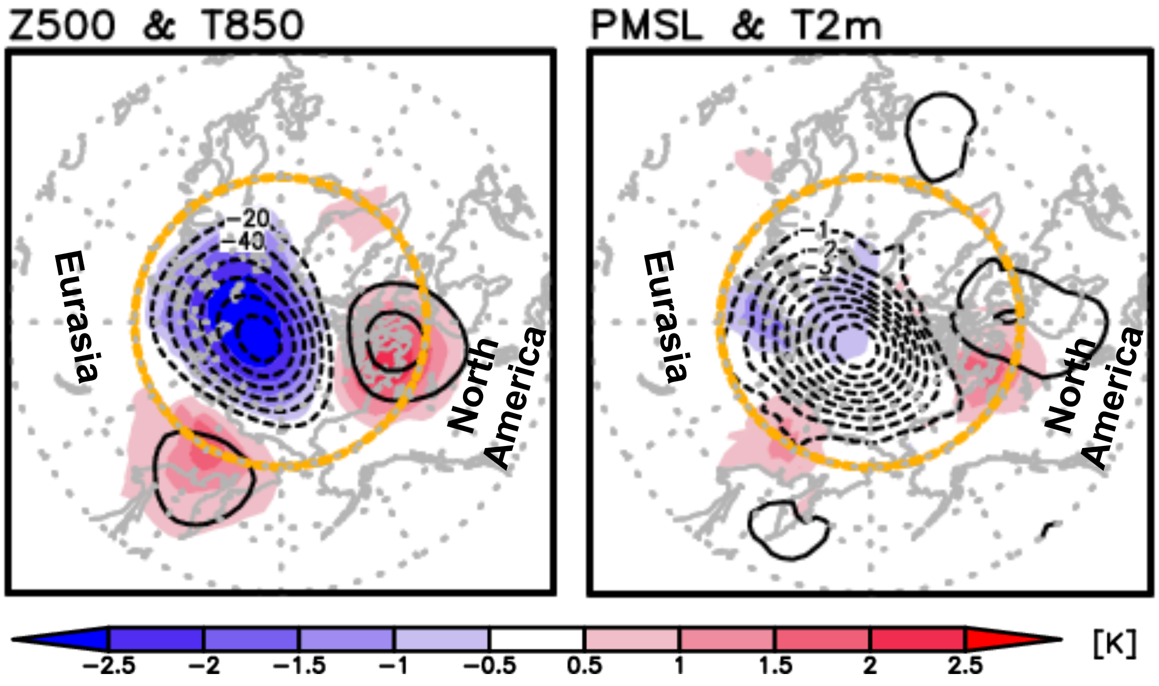

Contours: 500-hPa geopotential height anomalies

Shading: 850-hPa temperature anomalies

Contours: Sea level pressure (SLP) anomalies

Shading: 2-m temperature anomalies

Composites for "Arctic cyclone" pattern during June–September 1979–2019. Figure S2 adapted from Yamagami and Matsueda (2021).

- Yamagami and Matsueda (2021) suggest that forecast busts over the Arctic during summer may be linked to forecast errors in synoptic-scale systems such as ACs.

Literature review: Forecast skill over the Arctic

- Forecast errors propagating along upper-tropospheric waveguides and associated with features embedded within upper-tropospheric waveguides (e.g., Langland et al. 2002; Davies and Didione 2013; Baumgart et al. 2018) have been shown to contribute to forecast errors in the synoptic-scale flow over the middle latitudes.

- Forecast errors related to baroclinic processes (e.g.,Tribbia and Baumhefner 2004; Davies and Didone 2013) and latent heating (e.g., Rodwell et al. 2013; Martínez-Alvarado et al. 2016) have been shown to contribute to forecast errors in the synoptic-scale flow over the middle latitudes.

- Anticipate that the aforementioned forecast errors may contribute to forecast errors in the synoptic-scale flow over the Arctic.

Literature review: AC climatology

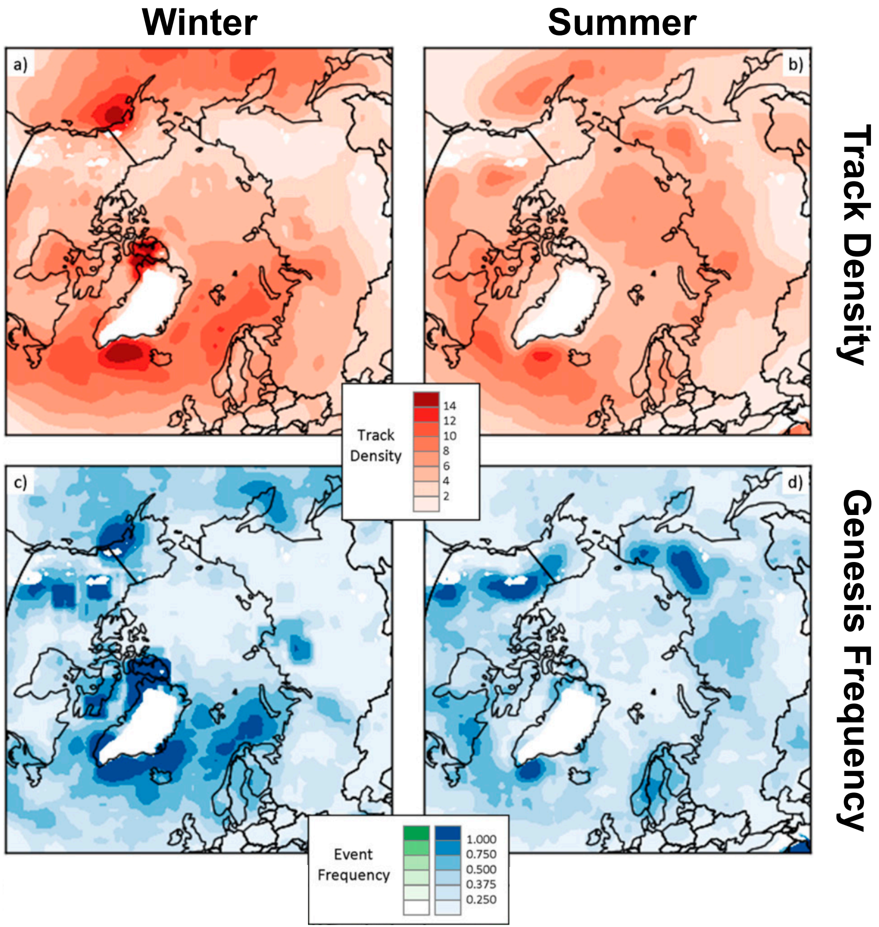

- ACs track most frequently over the North Atlantic and adjacent seas during winter.
- ACs track most frequently over Eurasia and adjacent seas, and the Arctic Ocean, during summer.
- AC genesis is most frequent over the North Atlantic and adjacent seas during winter.
- AC genesis is most frequent over Eurasia during summer.

Figure 3 adapted from Crawford et al. (2016).

Literature review: Features and processes influencing ACs

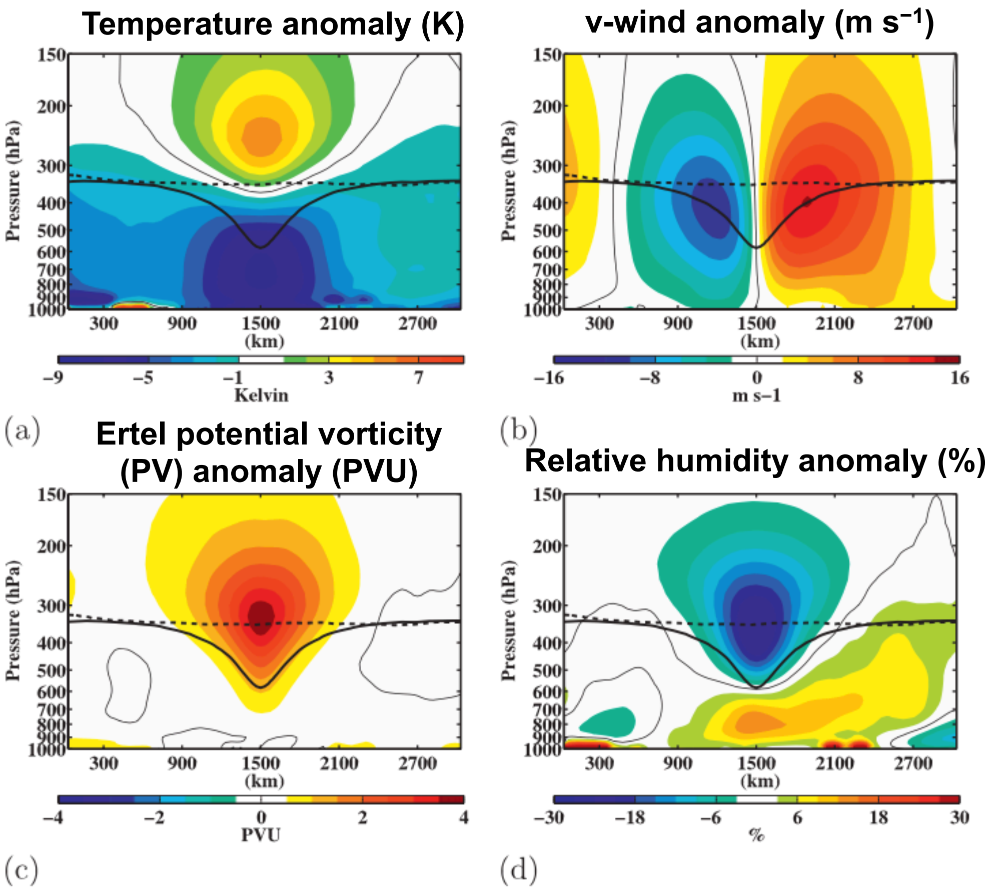

Composite west-to-east cross sections of TPVs. Figure 9 adapted from Cavallo and Hakim (2010).

- Tropopause polar vortices (TPVs) are coherent tropopause-based cyclonic vortices that occur frequently across the Arctic (e.g., Cavallo and Hakim 2009, 2010, 2012)

Literature review: Features and processes influencing ACs

- TPVs have been shown to play an important role in the development and intensification of ACs (e.g., Simmonds and Rudeva 2012, 2014; Tanaka et al. 2012; Aizawa and Tanaka 2016; Tao et al. 2017a,b; Yamagami et al. 2017).

- Baroclinic processes have also been shown to play an important role in the development and intensification of ACs (e.g., Simmonds and Rudeva 2012; Aizawa et al. 2014; Tao et al. 2017a,b; Yamagami et al. 2017).

Literature review: Features and processes influencing ACs

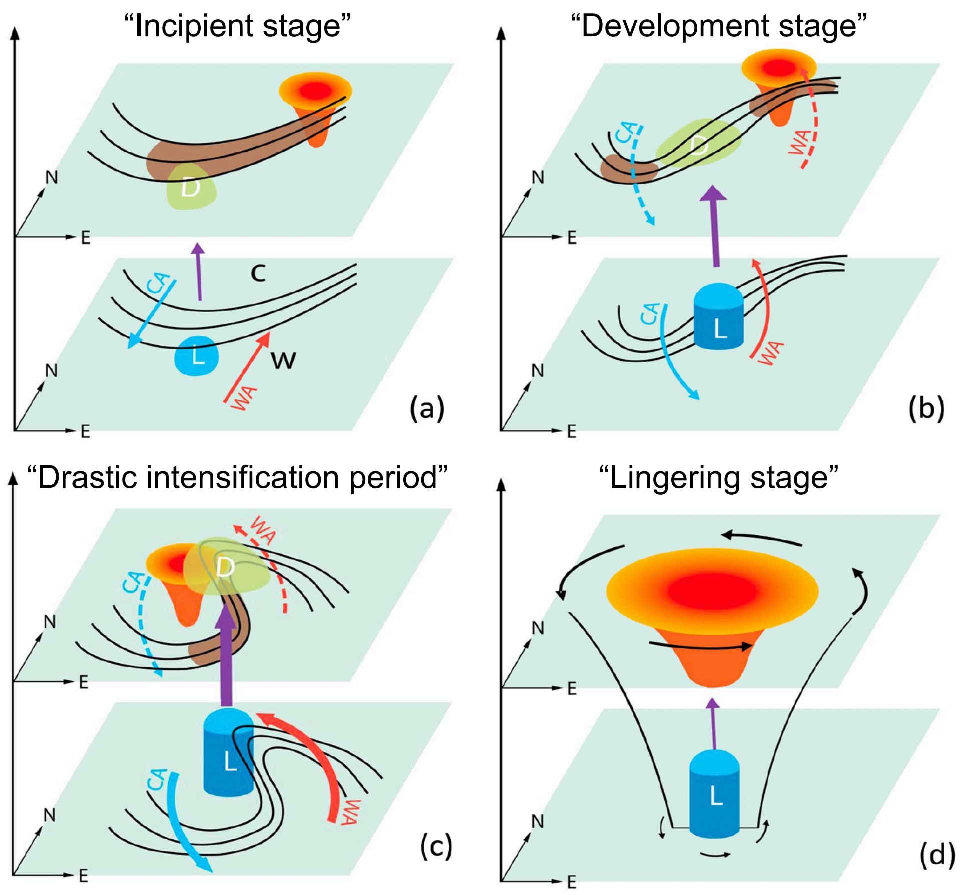

Sketch of the development of the Great Arctic Cyclone of August 2012 (AC12). Figure 4 adapted from Tao et al. (2017b).

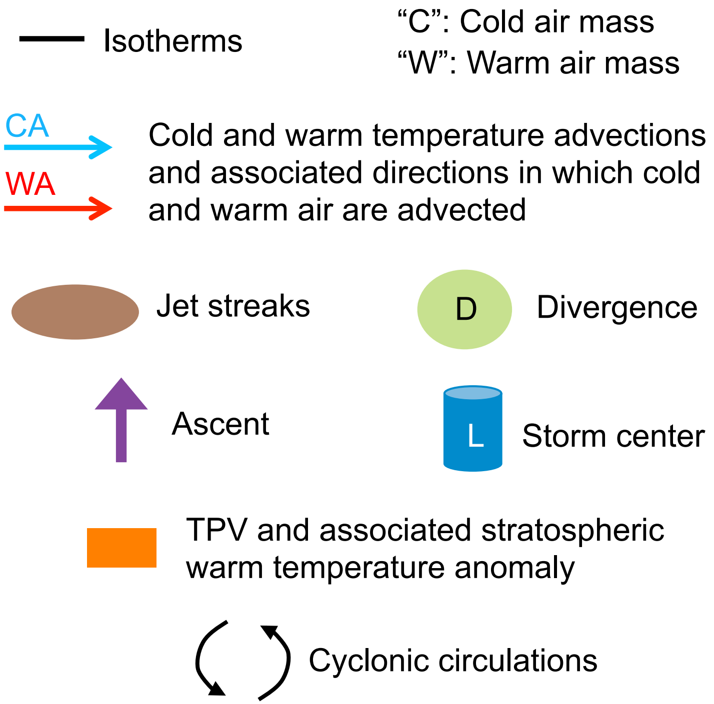

Literature review: Features and processes influencing ACs

- Latent heating has been shown to contribute to the development and intensification of midlatitude cyclones in numerous studies (e.g., Tracton 1973; Kuo and Reed 1988; Davis et al. 1993; Stoelinga 1996; Wernli et al. 2002).

- There has been a dearth of research that has examined the role of latent heating in the development and intensification of ACs.

- ACs can be associated with intrusions of warm, moist air into the Arctic (e.g., Binder et al. 2017; Messori et al. 2018; Fearon et al. 2021), which correspond to atmospheric rivers (ARs) and warm conveyor belts (WCBs).

Literature review: Forecast skill of ACs

- The forecast skill of AC12 has been shown to be sensitive to the strength of TPVs (e.g., Tao et al. 2017b; Yamazaki et al. 2015), the position of TPVs (e.g., Yamagami et al. 2018a), and the strength of tropospheric baroclinicity (e.g.,Tao et al. 2017b).

- Johnson and Wang (2021) find that track and intensity errors of an AC during July 2018 are sensitive to the position and intensity of TPVs, the amount of midtropospheric moisture located within the WCB associated with the AC, and the structure of the lower-tropospheric thermal field.

Literature review: Forecast skill of ACs

- Yamagami et al. (2019) and Capute and Torn (2021) show that ACs with lower forecast skill of intensity tend to be stronger.

- Capute and Torn (2021) find that low-skill ACs are typically embedded in regions of larger lower-to-midtropospheric Eady growth rates compared to high-skill ACs, but find no systematic difference in latent heating between low-skill ACs and high-skill ACs.

Hypotheses

1) The Arctic environment tends to be characterized by greater synoptic-scale flow amplitude, greater baroclinic growth rates, and greater latent heating during low-skill periods compared to high-skill periods.

Hypotheses

1) The Arctic environment tends to be characterized by greater synoptic-scale flow amplitude, greater baroclinic growth rates, and greater latent heating during low-skill periods compared to high-skill periods.

2) ACs occur more frequently across the Arctic, tend to be stronger, and tend to be embedded in more favorable dynamic and thermodynamic environments for development and intensification during low-skill periods compared to high-skill periods.

Hypotheses

3) TPVs, baroclinic zones, and WCBs, and TPV–AC interactions, baroclinic processes, and latent heating, influence the evolution of strong low-skill ACs during low-skill periods.

Hypotheses

3) TPVs, baroclinic zones, and WCBs, and TPV–AC interactions, baroclinic processes, and latent heating, influence the evolution of strong low-skill ACs during low-skill periods.

4) Forecast errors in TPVs, baroclinic zones, and WCBs, and forecast errors in TPV–AC interactions, baroclinic processes, and latent heating, contribute to forecast errors in strong low-skill ACs during low-skill periods.

Hypotheses

1) The Arctic environment tends to be characterized by greater synoptic-scale flow amplitude, greater baroclinic growth rates, and greater latent heating during low-skill periods compared to high-skill periods.

2) ACs occur more frequently across the Arctic, tend to be stronger, and tend to be embedded in more favorable dynamic and thermodynamic environments for development and intensification during low-skill periods compared to high-skill periods.

Arctic forecast skill evaluation

- Utilize day-5 forecasts of 500-hPa geopotential height initialized at 0000 UTC during June–August 2007–2017 from 11-member 1° NOAA GEFS reforecast dataset version 2 (Hamill et al. 2013).

- Calculate area-averaged root mean square error (RMSE) of 500-hPa geopotential height over the Arctic, using ERA-Interim (Dee et al. 2011) at 1° horizontal resolution as verification.

- Calculate standardized anomaly of area-averaged RMSE (σ_{RMSE}) by following the approach used by Ben Moore [2017, section 5b(3)].

Arctic forecast skill evaluation

- Refer to forecasts associated with the top and bottom 10% of σ_{RMSE} at day 5 as **low-skill forecasts** and **high-skill forecasts**, respectively.
  - There are 101 low-skill forecasts and 101 high-skill forecasts.
- Refer to time periods extending from day 0 through day 5 that are encompassed by low-skill forecasts and high-skill forecasts as **low-skill periods** and **high-skill periods**, respectively.
- If a day occurs during both a low-skill period and a high-skill period, the day is assigned to the period that occurs earlier.

Identification of ACs

- Create a climatology of ACs occurring during June–August 2007–2017 by obtaining cyclone tracks from 1° ERA-Interim cyclone climatology prepared by Sprenger et al. (2017).

- Deem cyclones that last ≥ 48 h and spend at least 6 h poleward of 70°N as ACs.

- Identify ACs that occur at any time during low-skill periods and high-skill periods.

Characteristics of the Arctic environment and ACs

- Calculate selected dynamic and thermodynamic quantities to characterize the Arctic environment and ACs using ERA-Interim at 1° horizontal resolution.

- Area-average the selected quantities over the Arctic ($\geq$ 70°N) to characterize the Arctic environment.

- Area-average the selected quantities within a 1000-km radius from the center of each AC to characterize the environment in the vicinity of each AC.

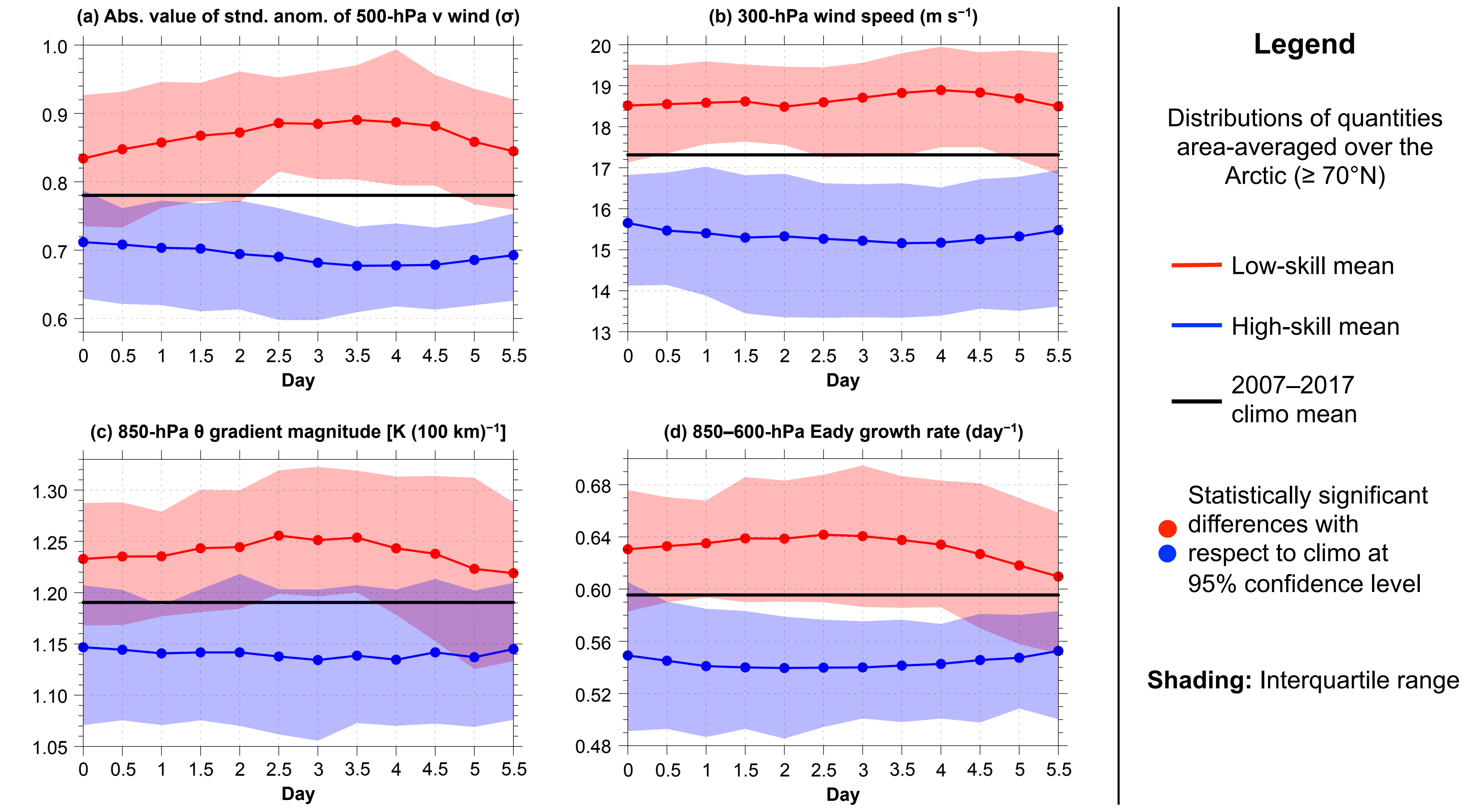
(a) Abs. value of stnd. anom. of 500-hPa v wind (σ)
1.0
0.9
0.8
0.7
0.6
0 0.5 1 1.5 2 2.5 3 3.5 4 4.5 5 5.5
Day
(b) 300-hPa wind speed (m s⁻¹)
20
19
18
17
16
15
14
13
0 0.5 1 1.5 2 2.5 3 3.5 4 4.5 5 5.5
Day
(c) 850-hPa θ gradient magnitude [K (100 km)⁻¹]
1.30
1.25
1.20
1.15
1.10
1.05
0 0.5 1 1.5 2 2.5 3 3.5 4 4.5 5 5.5
Day
(d) 850–600-hPa Eady growth rate (day⁻¹)
0.68
0.64
0.60
0.56
0.52
0.48
0 0.5 1 1.5 2 2.5 3 3.5 4 4.5 5 5.5
Day
Legend
Distributions of quantities area-averaged over the Arctic (≥ 70°N)
Low-skill mean
High-skill mean
2007–2017 climo mean
Statistically significant differences with respect to climo at 95% confidence level
Shading: Interquartile range

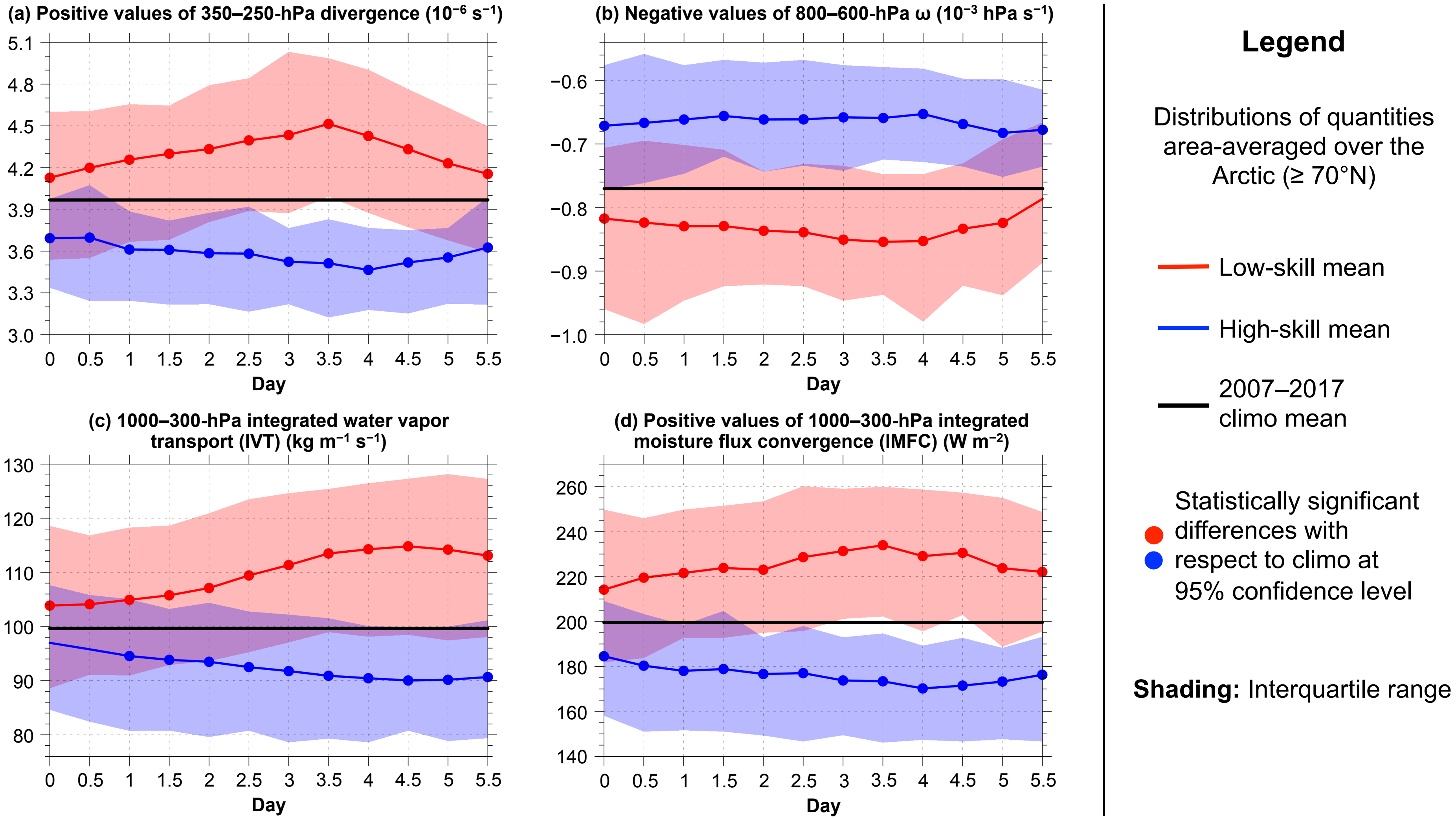
(a) Positive values of 350–250-hPa divergence (10⁻⁶ s⁻¹)
(b) Negative values of 800–600-hPa ω (10⁻³ hPa s⁻¹)
(c) 1000–300-hPa integrated water vapor transport (IVT) (kg m⁻¹ s⁻¹)
(d) Positive values of 1000–300-hPa integrated moisture flux convergence (IMFC) (W m⁻²)
Day
Legend
Distributions of quantities area-averaged over the Arctic (≥ 70°N)
Low-skill mean
High-skill mean
2007–2017 climo mean
Statistically significant differences with respect to climo at 95% confidence level
Shading: Interquartile range

AC track frequency

ACs during low-skill periods (*N* = 298) | **ACs during high-skill periods (*N* = 208)** | **Low-skill periods minus high-skill periods**

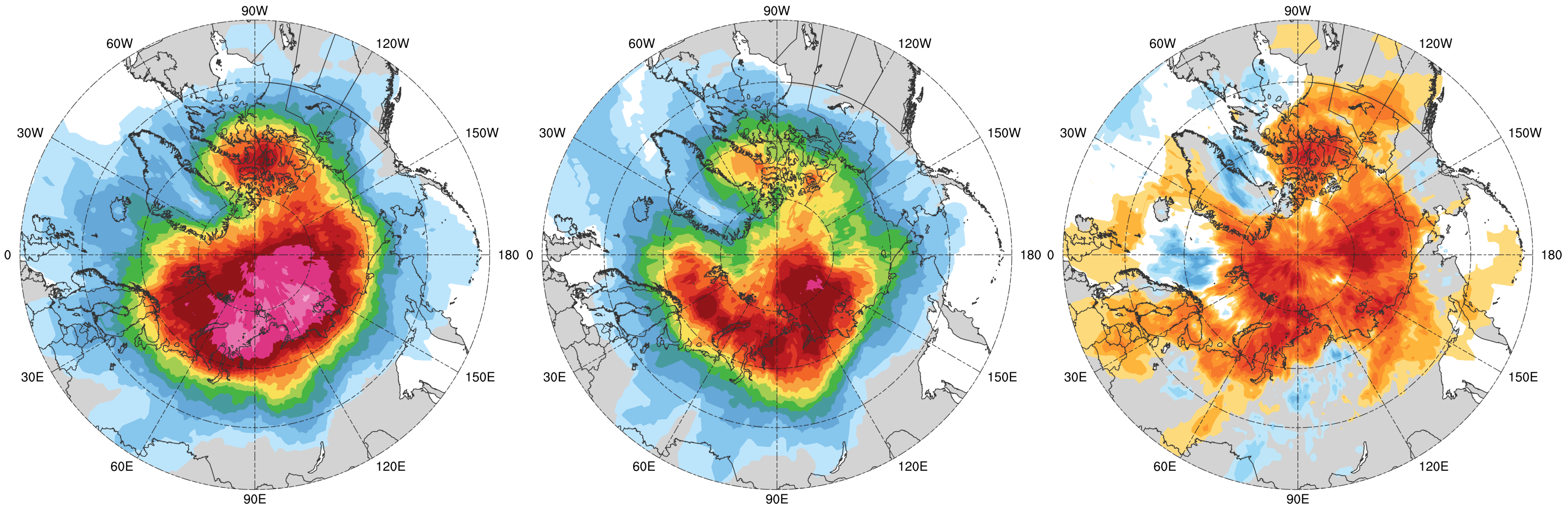

AC track frequency: Number of ACs within 500 km of a grid point, normalized by number of days in period (number of ACs day^{-1})

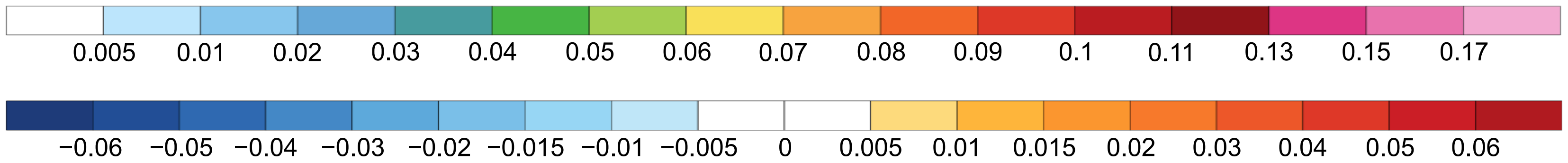

AC characteristics

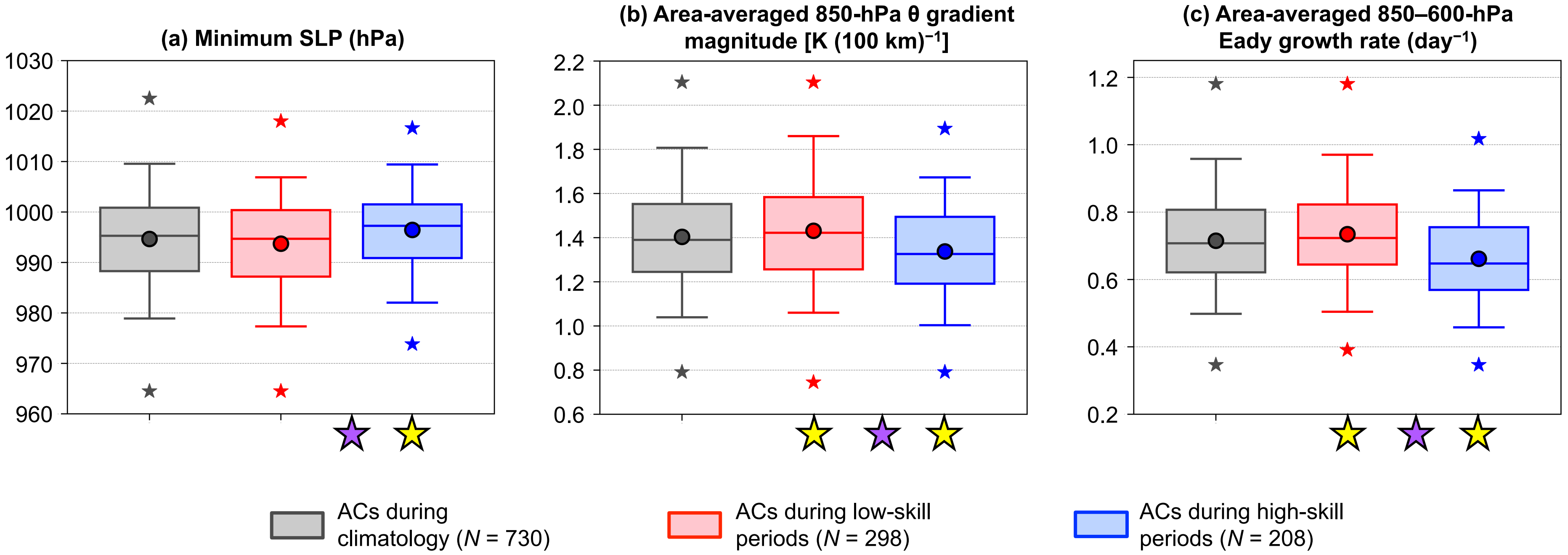

Distributions of most extreme value of quantities characterizing ACs when ACs are located in the Arctic during the periods of interest.

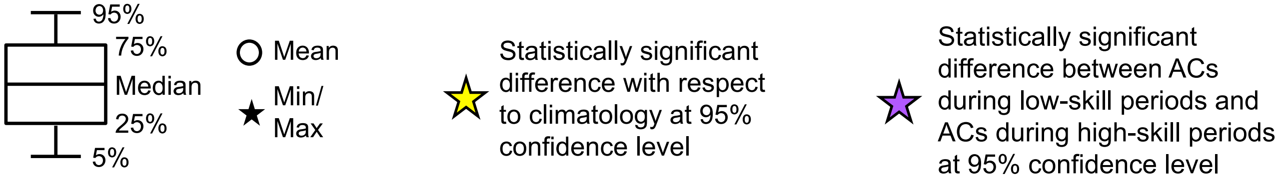

AC characteristics

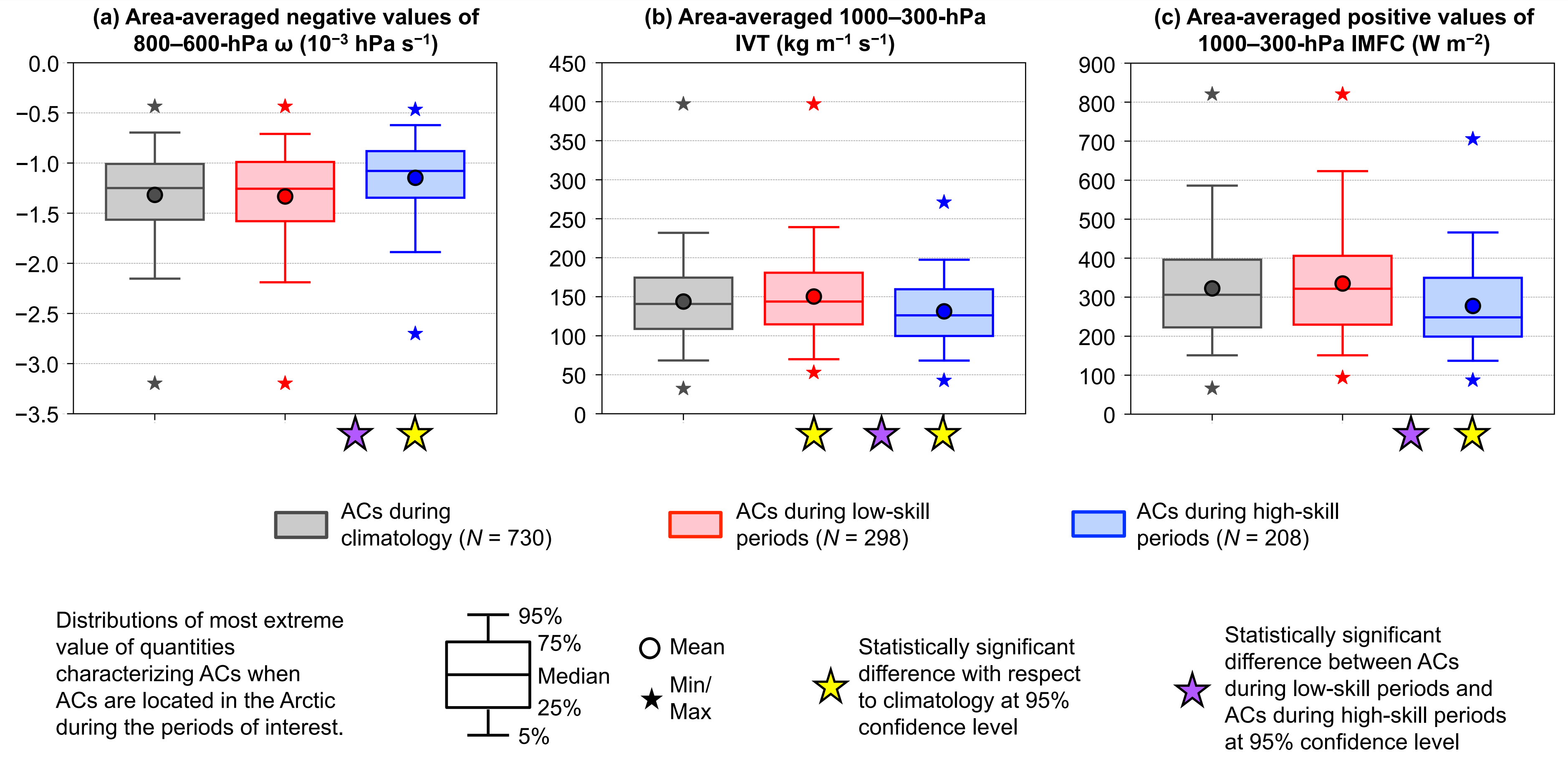

Hypotheses

3) TPVs, baroclinic zones, and WCBs, and TPV–AC interactions, baroclinic processes, and latent heating, influence the evolution of strong low-skill ACs during low-skill periods.

Determining strong low-skill ACs

- Track ACs during low-skill periods in forecasts from NOAA GEFS reforecast dataset version 2 by utilizing an objective SLP-based cyclone tracking algorithm developed by Crawford et al. (2020).
- Consider forecasts initialized 5 days prior to the 0000 UTC time of lowest SLP of the ACs when located in the Arctic (> 70°N) during low-skill periods (verification time).
- Adapt methodology of Korfe and Colle (2018) to identify ACs in the forecasts that match the ACs during low-skill periods.

Determining strong low-skill ACs

- Calculate day-5 intensity RMSE at the verification time, considering only ACs during low-skill periods for which there are ≥ 5 ensemble members with a matching AC occurring at the verification time.

- Refer to ACs during low-skill periods associated with the top 25% of day-5 intensity RMSE as low-skill ACs during low-skill periods.

Determining strong low-skill ACs

- Determine top 25% strongest low-skill ACs during low-skill periods based on the lowest SLP attained by these ACs when located in the Arctic (> 70°N) during low-skill periods.
  - These ACs are hereafter referred to as strong low-skill ACs.
- Track the strong low-skill ACs using ERA5 (Hersbach et al. 2020) at 0.25° horizontal resolution, every 6 h.
- Construct AC-centered composites for the strong low-skill ACs at various lag times relative to the time of lowest SLP of these ACs when located in the Arctic (t_{low}) using ERA5 at 0.25° horizontal resolution.

Strong low-skill ACs

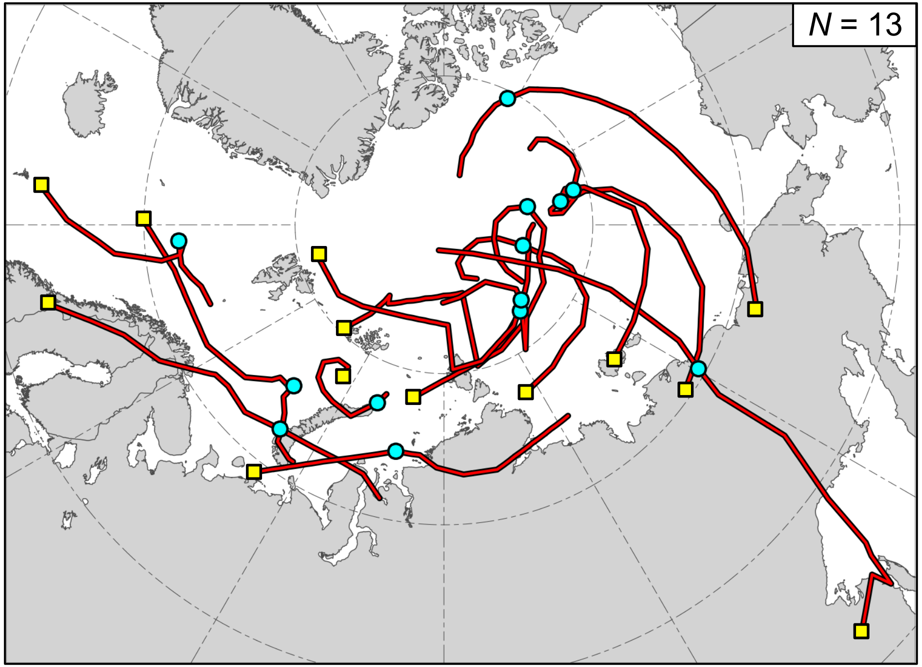

AC location at earliest valid lag hour

AC location at t_{low}

Red lines show tracks of ACs during lag hours of –48 to +36 h, every 6 h, relative to t_{low}, when valid

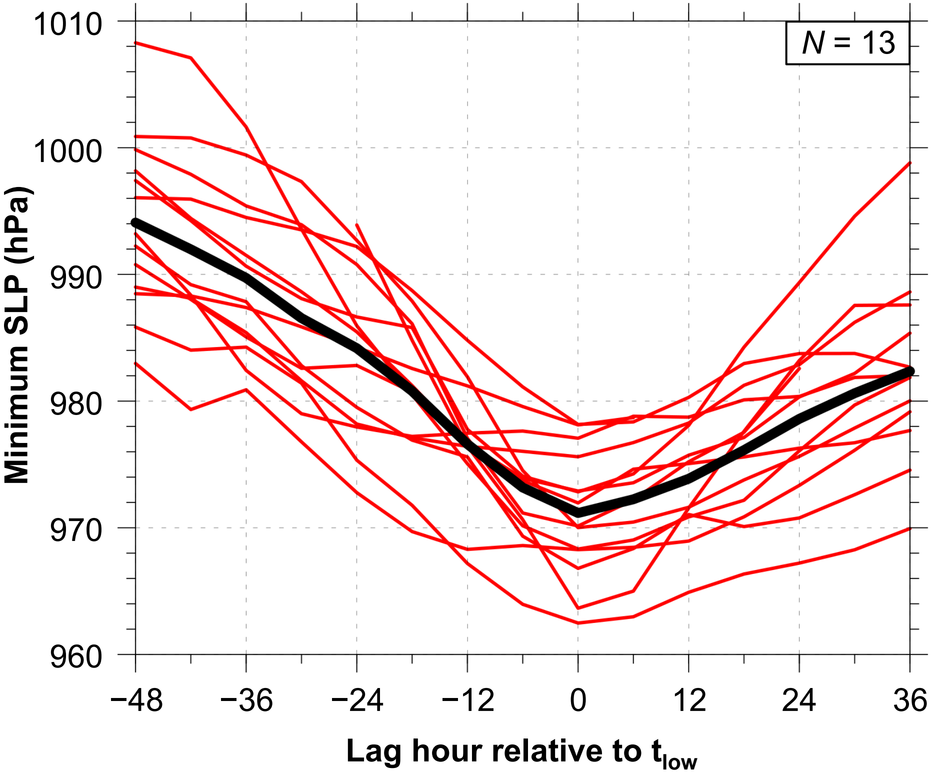

Time series of minimum SLP (hPa) of ACs (red) and of mean minimum SLP (hPa) of ACs (black) during lag hours of –48 to +36 h, every 6 h, relative to t_{low}, when valid

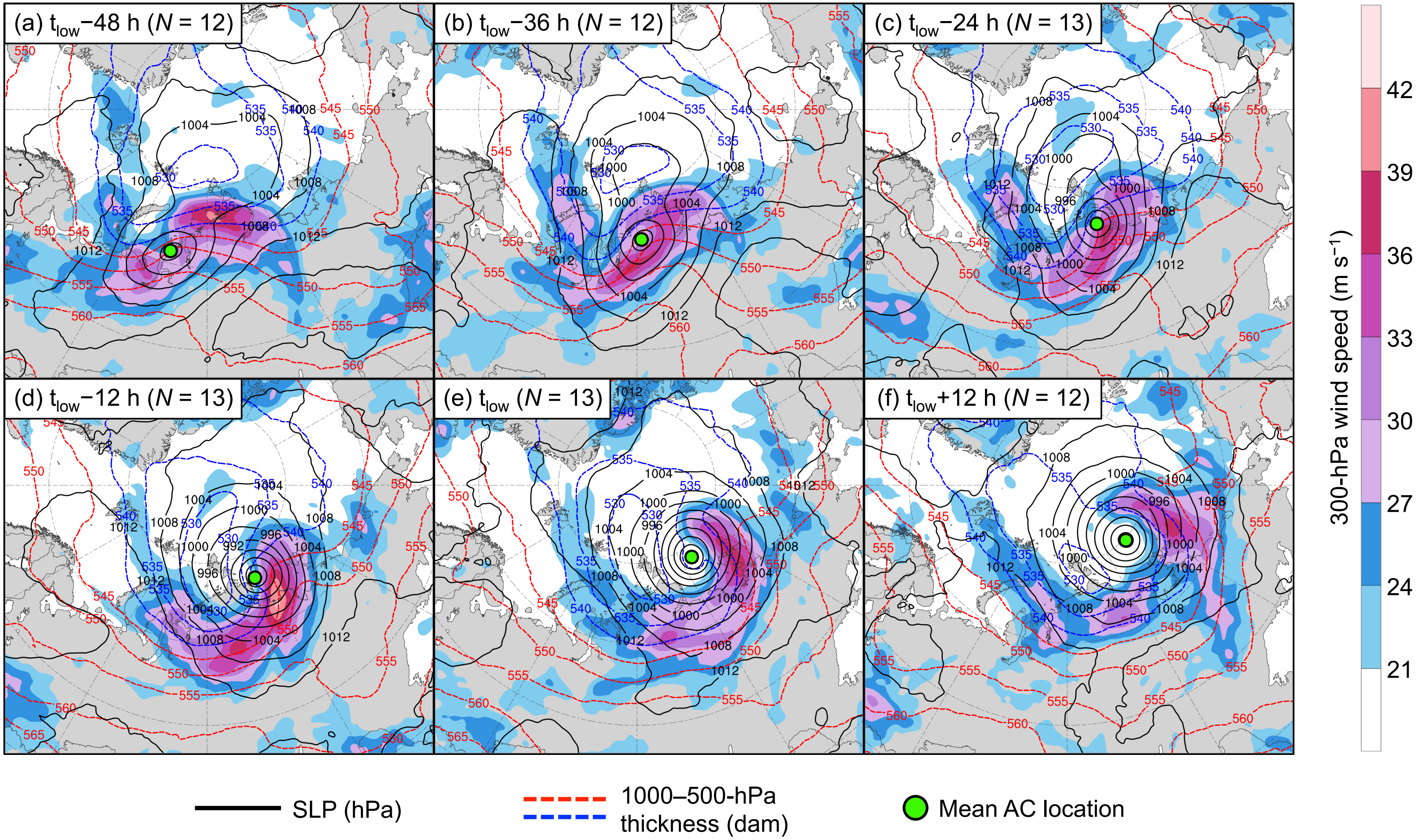

(a) t_low−48 h (N = 12)
(b) t_low−36 h (N = 12)
(c) t_low−24 h (N = 13)
(d) t_low−12 h (N = 13)
(e) t_low (N = 13)
(f) t_low+12 h (N = 12)
300-hPa wind speed (m s−1)
42
39
36
33
30
27
24
21
SLP (hPa)
1000–500-hPa thickness (dam)
Mean AC location

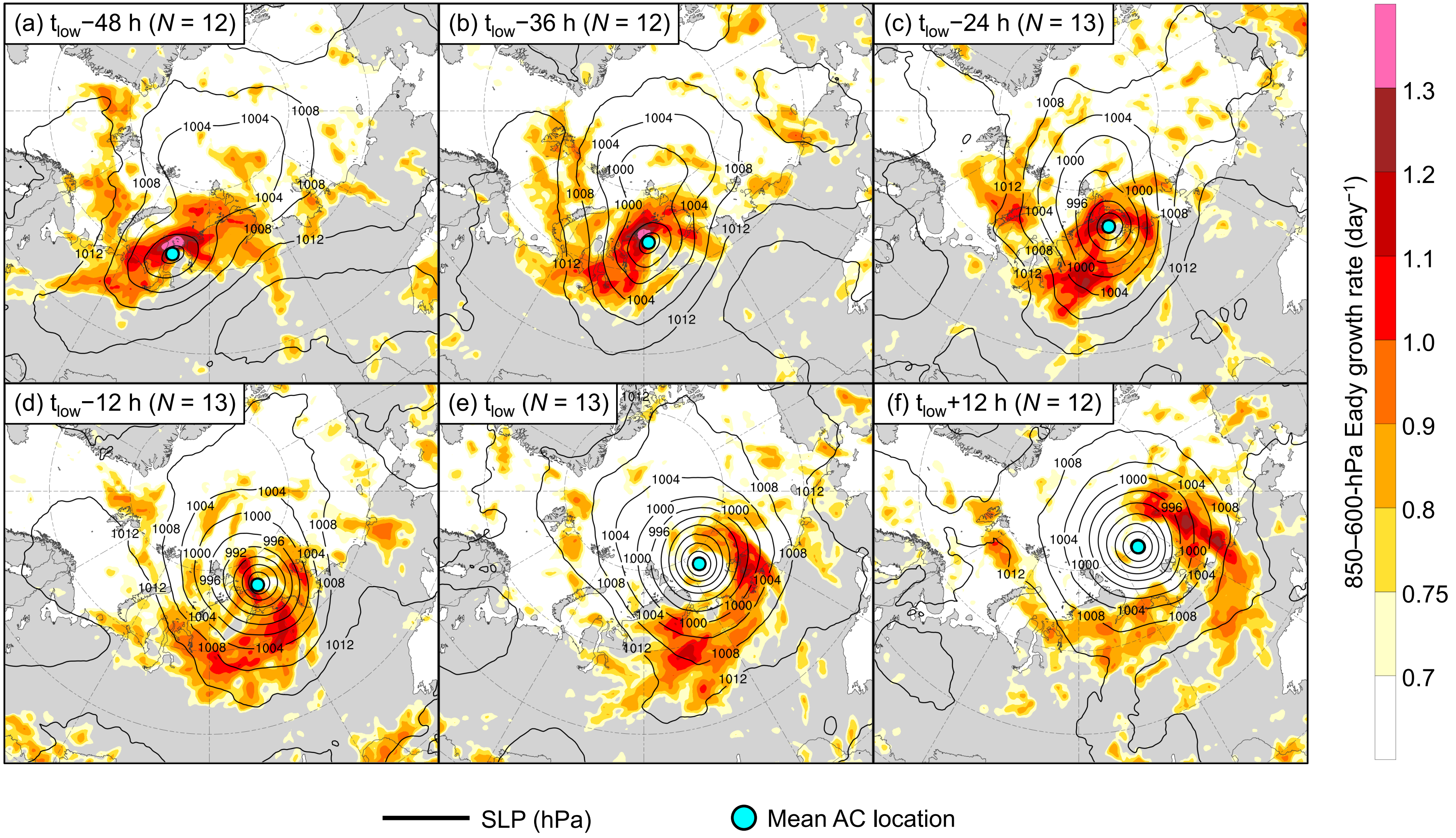
(a) t_low−48 h (N = 12)
(b) t_low−36 h (N = 12)
(c) t_low−24 h (N = 13)
(d) t_low−12 h (N = 13)
(e) t_low (N = 13)
(f) t_low+12 h (N = 12)
850–600-hPa Eady growth rate (day⁻¹)
1.3
1.2
1.1
1.0
0.9
0.8
0.75
0.7
SLP (hPa)
Mean AC location

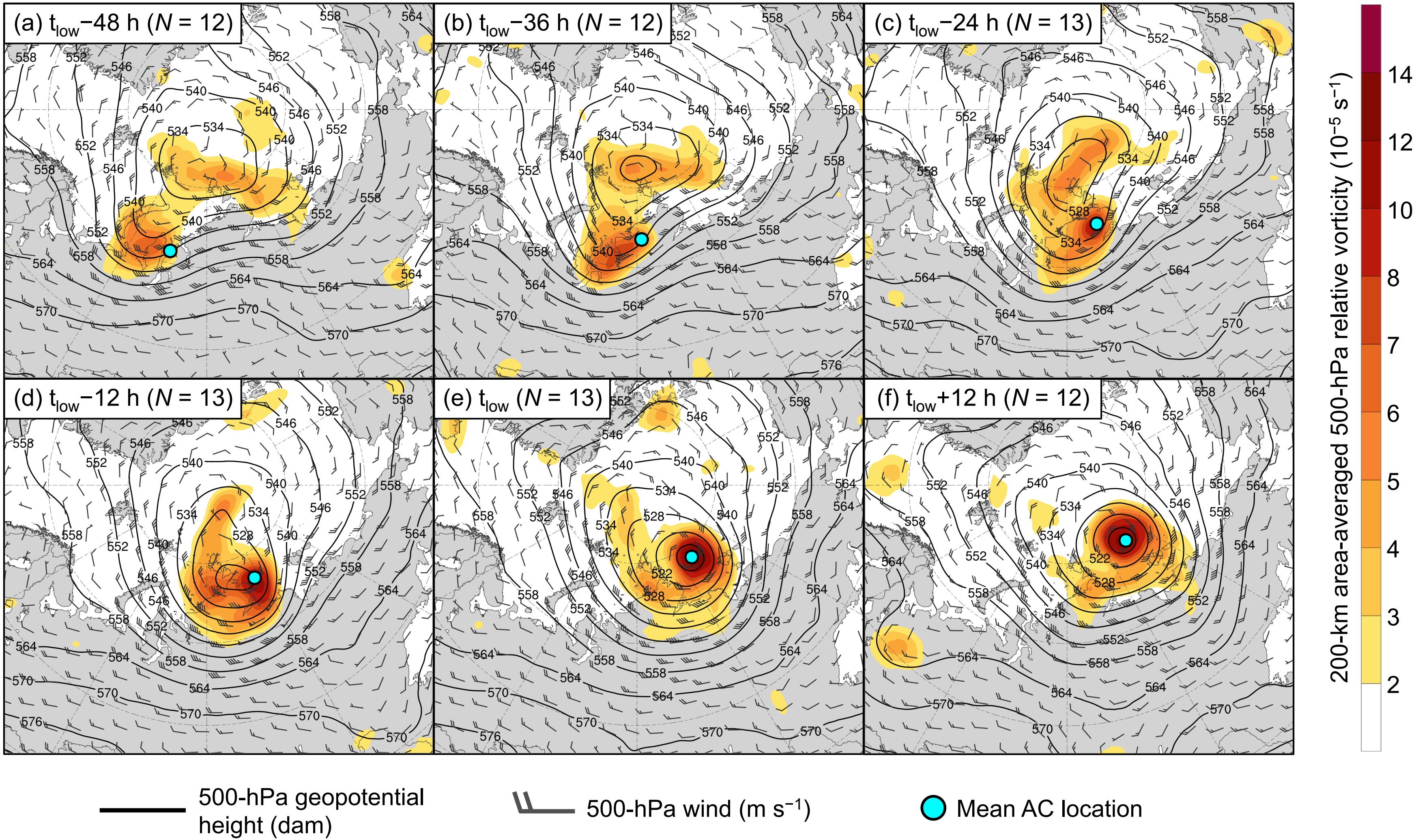
(a) t_{low}−48 h (N = 12)
(b) t_{low}−36 h (N = 12)
(c) t_{low}−24 h (N = 13)
(d) t_{low}−12 h (N = 13)
(e) t_{low} (N = 13)
(f) t_{low}+12 h (N = 12)
200-km area-averaged 500-hPa relative vorticity (10^{-5} s^{-1})
2
3
4
5
6
7
8
10
12
14
500-hPa geopotential height (dam)
500-hPa wind (m s^{-1})
Mean AC location

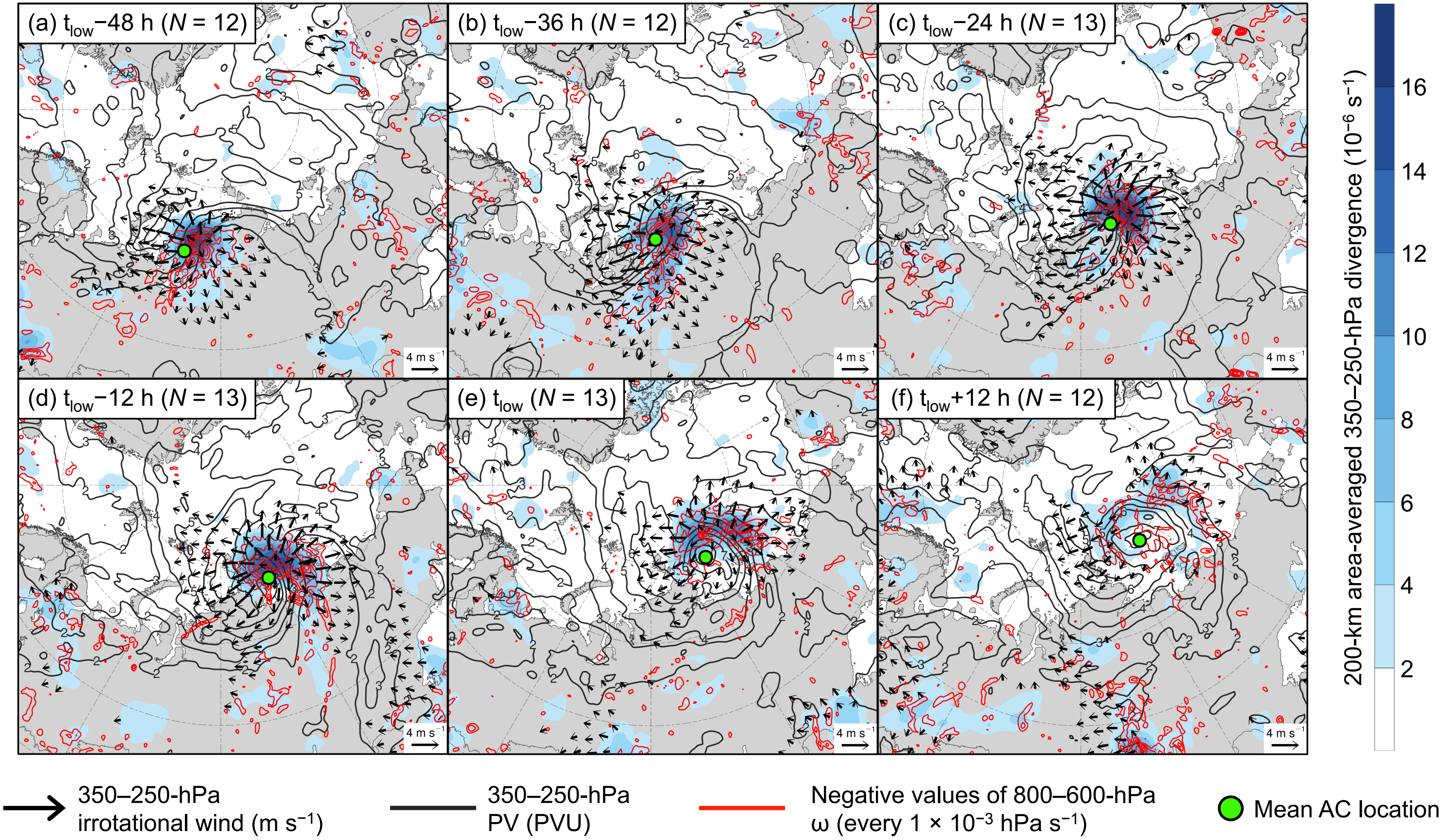

(a) t_{low}−48 h (N = 12)
(b) t_{low}−36 h (N = 12)
(c) t_{low}−24 h (N = 13)
(d) t_{low}−12 h (N = 13)
(e) t_{low} (N = 13)
(f) t_{low}+12 h (N = 12)
4 m s^{-1}
200-km area-averaged 350–250-hPa divergence (10^{-6} s^{-1})
2
4
6
8
10
12
14
16
350–250-hPa irrotational wind (m s^{-1})
350–250-hPa PV (PVU)
Negative values of 800–600-hPa ω (every 1 × 10^{-3} hPa s^{-1})
Mean AC location

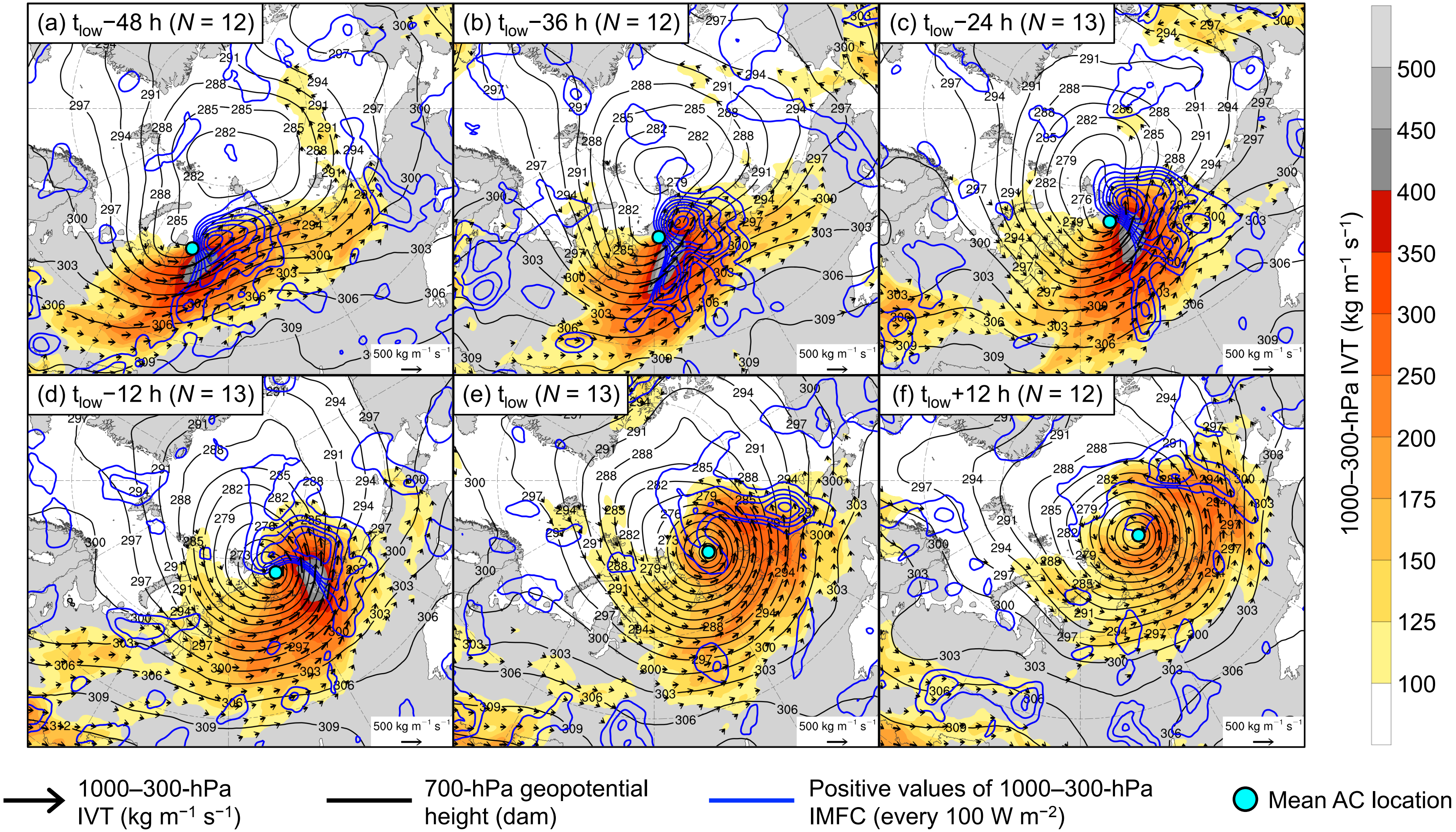
(a) t_{low}−48 h (N = 12)
(b) t_{low}−36 h (N = 12)
(c) t_{low}−24 h (N = 13)
(d) t_{low}−12 h (N = 13)
(e) t_{low} (N = 13)
(f) t_{low}+12 h (N = 12)
500 kg m^{-1} s^{-1}
1000–300-hPa IVT (kg m^{-1} s^{-1})
500
450
400
350
300
250
200
175
150
125
100
1000–300-hPa IVT (kg m^{-1} s^{-1})
700-hPa geopotential height (dam)
Positive values of 1000–300-hPa IMFC (every 100 W m^{-2})
Mean AC location

Hypotheses

4) Forecast errors in TPVs, baroclinic zones, and WCBs, and forecast errors in TPV–AC interactions, baroclinic processes, and latent heating, contribute to forecast errors in strong low-skill ACs during low-skill periods.

Case selection

- Selected a strong low-skill AC that occurred during 13–19 August 2016 (AC16), which is a representative member of the strong low-skill ACs.

AC16 track and intensity

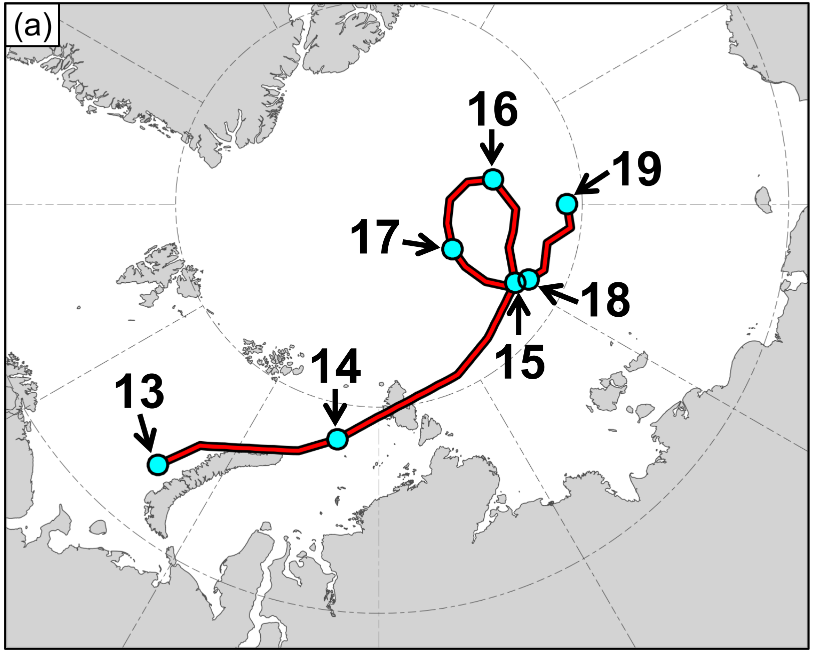

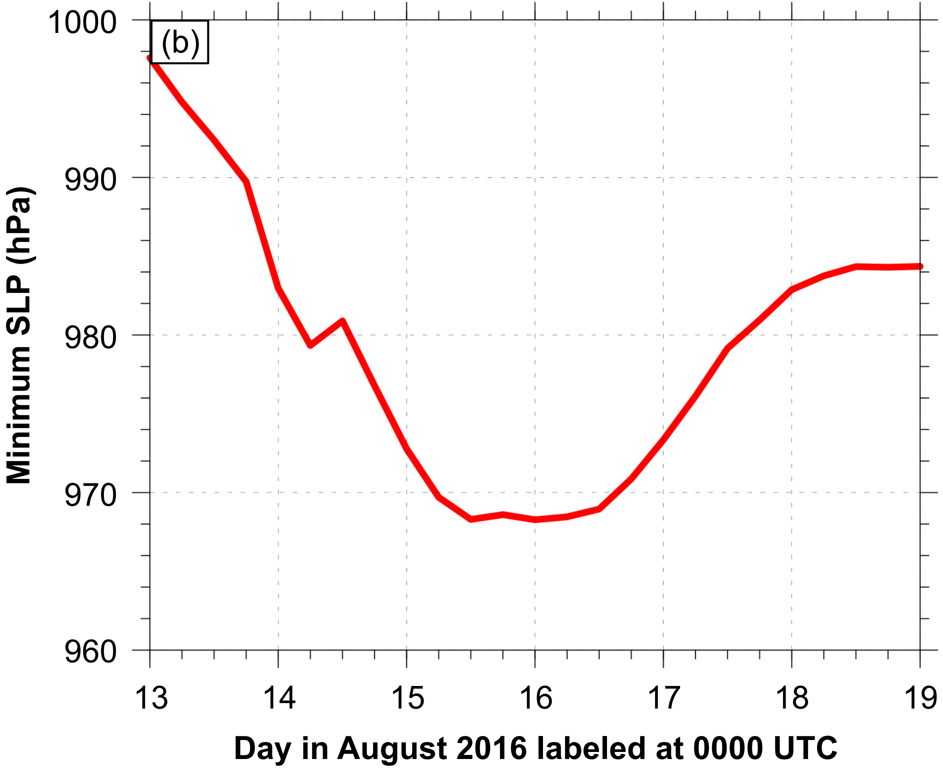

0000 UTC positions of AC16

Red line shows track of AC16 during 13–19 Aug 2016. Numbers represent dates of 0000 UTC positions of AC.

Time series of minimum SLP (hPa) of AC16 during 13–19 Aug 2016.

Data source: ERA5

AC16 in ECMWF EPS

- Use ensemble forecasts from the 51-member ECMWF EPS extracted from The Observing System Research and Predictability Experiment (THORPEX) Interactive Grand Global Ensemble (TIGGE) (Bougeault et al. 2010).

- Use ensemble forecasts initialized at 0000 UTC 10 August and verifying at 0000 UTC 15 August (120 h).

AC16 in ECMWF EPS

- Track AC16 in the ensemble forecasts by utilizing the objective SLP-based cyclone tracking algorithm developed by Crawford et al. (2020).

- Adapt methodology of Korfe and Colle (2018) to identify the AC that matches AC16 in each ensemble forecast.

- If no AC is identified to match AC16 in an ensemble forecast, AC16 is manually identified and tracked in the ensemble forecast.

Ensemble-based sensitivity analysis (ESA)

- Utilize ensemble-based sensitivity analysis (ESA) technique (e.g., Torn and Hakim 2008) to examine the sensitivity of the forecast skill of intensity and position of AC16 to selected dynamic and thermodynamic quantities at earlier forecast lead times.

- Calculate the sensitivity of a forecast metric of interest *J* to a model state variable x_i at an earlier forecast lead time for an ensemble of size M via

$$\frac{\partial J}{\partial x_i} = \frac{\mathrm{cov}(\mathbf{J},\ \mathbf{x}_i)}{\mathrm{var}(\mathbf{x}_i)}$$

- **J** and $\mathbf{x}_i$ denote the 1 × M ensemble estimates of the forecast metric and *i*th model state variable, respectively, cov denotes the covariance, and var denotes the variance (e.g., Torn and Hakim 2008).

Ensemble-based sensitivity analysis (ESA)

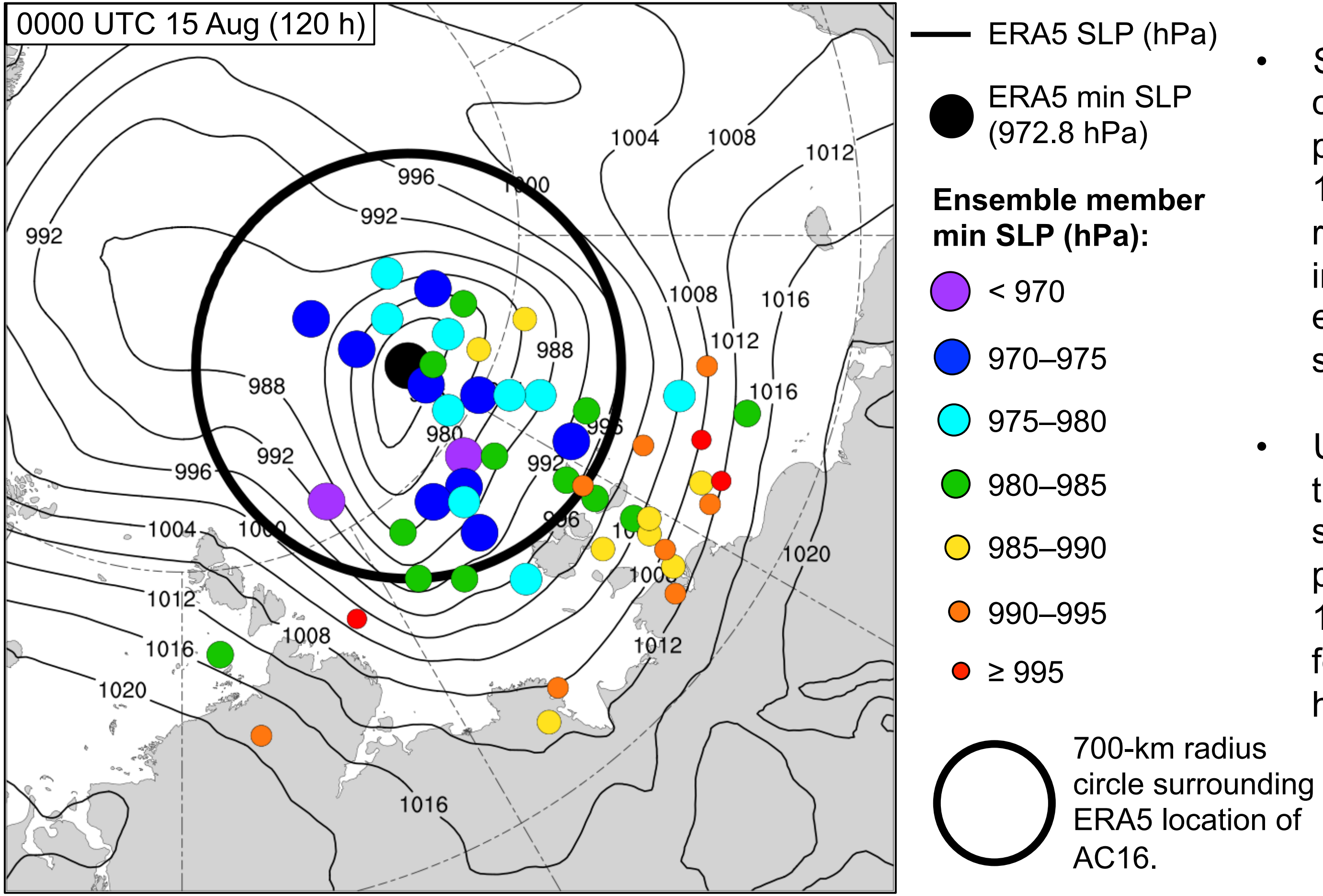

- SLP within a 700-km radius circle surrounding the ERA5 position of AC16 at 0000 UTC 15 August (120 h) correlates relatively well with the intensity error and position error of AC16 at this time (not shown).
- Use average SLP within the 700-km radius circle surrounding the ERA5 position of AC16 at 0000 UTC 15 August (120 h) as the forecast metric, which is hereafter referred to as J_{AC}.

Interpreting sensitivity values

- All sensitivity values are multiplied by −1, such that a more accurate prediction of the intensity and position of AC16 at 0000 UTC 15 August (120 h) is associated with increasing the value of the quantity for positive sensitivity values and with decreasing the value of the quantity for negative sensitivity values.

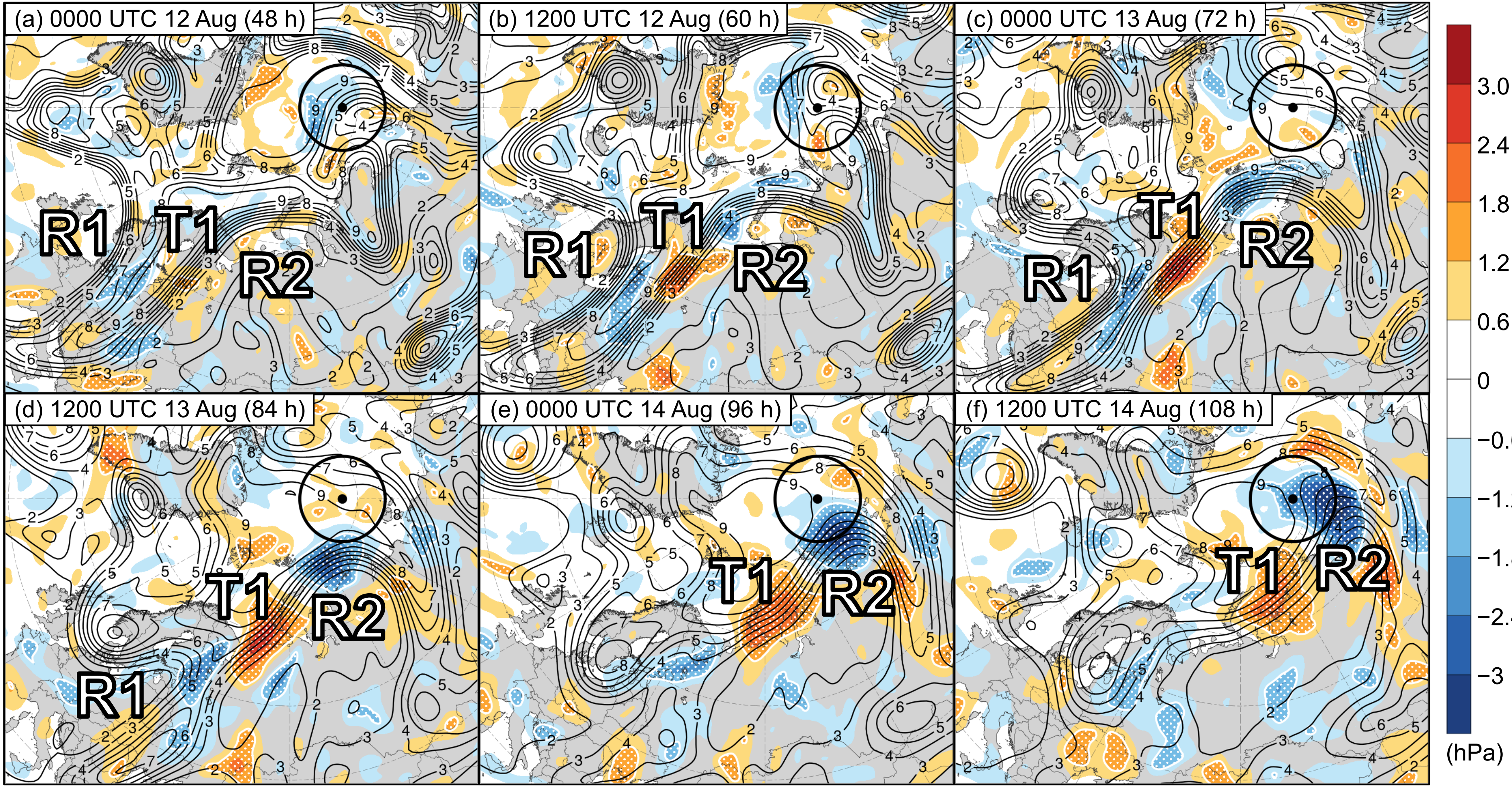

Ensemble mean 200-km area-averaged 250-hPa PV (PVU)

Shading: Sensitivity of J_{AC} to 200-km area-averaged 250-hPa PV (hPa)

White stippling: Sensitivity is statistically significant at 95% confidence level

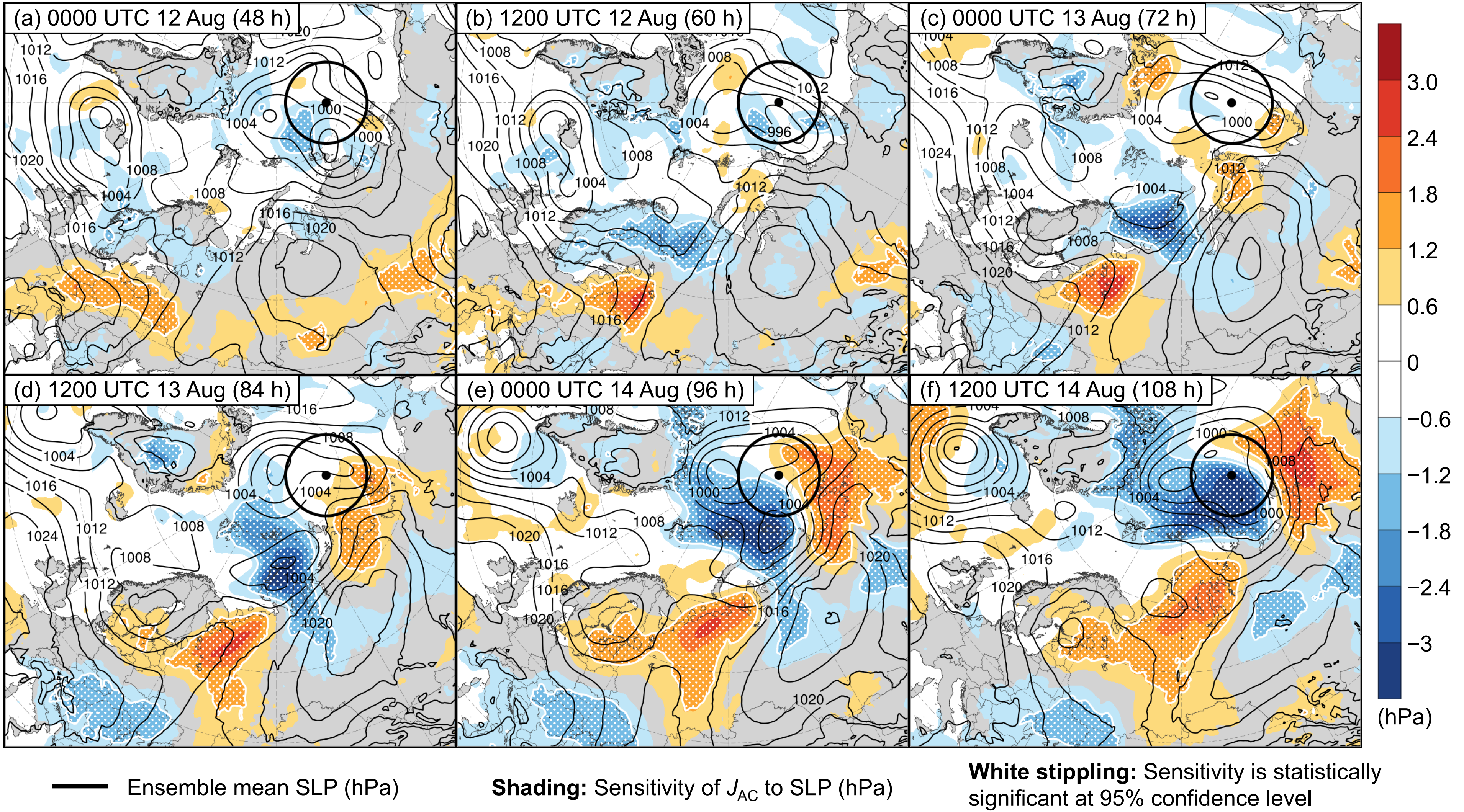

(a) 0000 UTC 12 Aug (48 h)
(b) 1200 UTC 12 Aug (60 h)
(c) 0000 UTC 13 Aug (72 h)
(d) 1200 UTC 13 Aug (84 h)
(e) 0000 UTC 14 Aug (96 h)
(f) 1200 UTC 14 Aug (108 h)
3.0
2.4
1.8
1.2
0.6
0
−0.6
−1.2
−1.8
−2.4
−3
(hPa)
Ensemble mean SLP (hPa)
Shading: Sensitivity of J_{AC} to SLP (hPa)
White stippling: Sensitivity is statistically significant at 95% confidence level

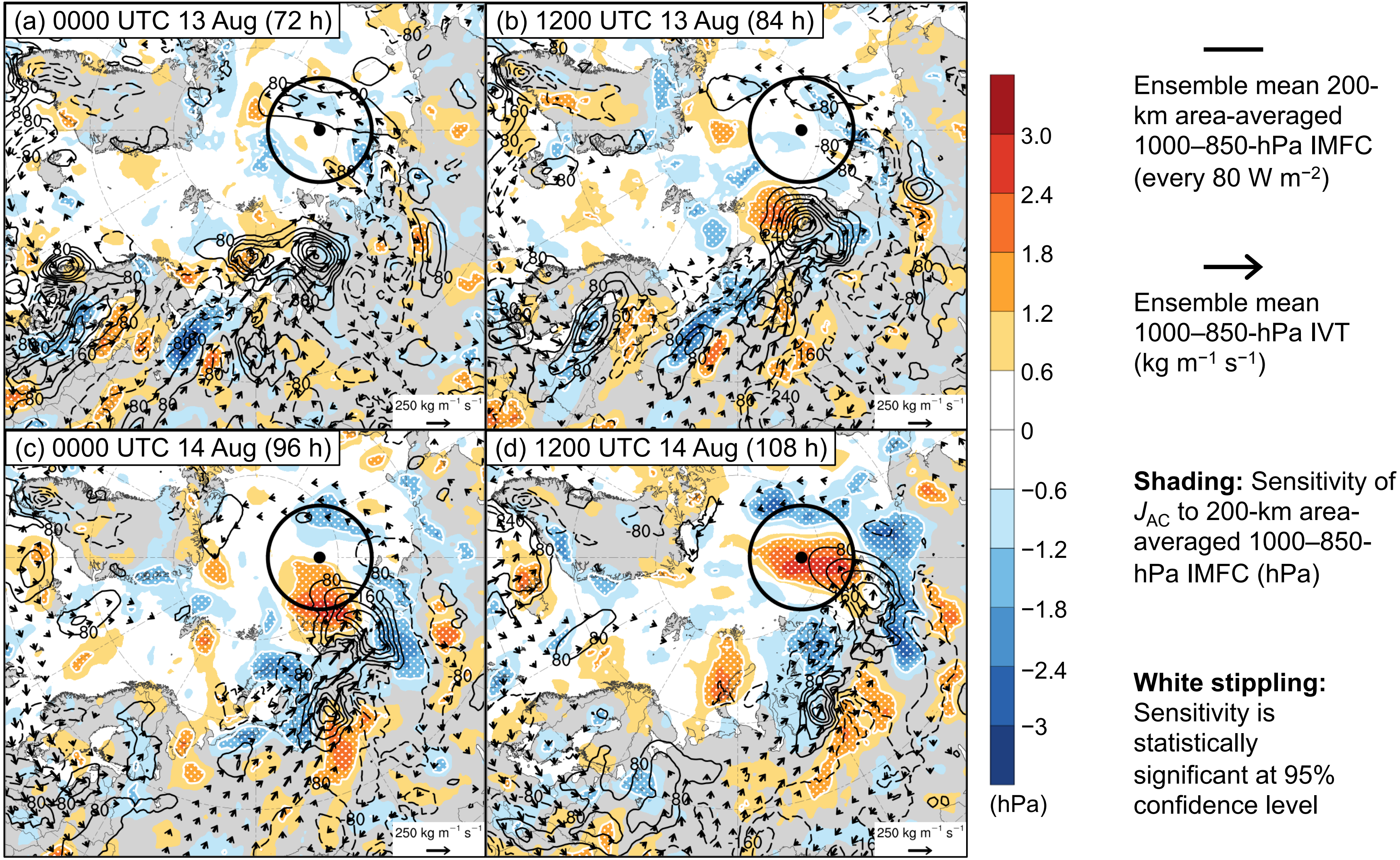

(a) 0000 UTC 13 Aug (72 h)
(b) 1200 UTC 13 Aug (84 h)
(c) 0000 UTC 14 Aug (96 h)
(d) 1200 UTC 14 Aug (108 h)
250 kg m⁻¹ s⁻¹
3.0
2.4
1.8
1.2
0.6
0
−0.6
−1.2
−1.8
−2.4
−3
(hPa)
Ensemble mean 200-km area-averaged 1000–850-hPa IMFC (every 80 W m⁻²)
Ensemble mean 1000–850-hPa IVT (kg m⁻¹ s⁻¹)
Shading: Sensitivity of J_AC to 200-km area-averaged 1000–850-hPa IMFC (hPa)
White stippling: Sensitivity is statistically significant at 95% confidence level

Summary

- The Arctic environment tends to be characterized by greater synoptic-scale flow amplitude, greater lower-to-midtropospheric Eady growth rates, greater moisture transport, and greater latent heating during low-skill periods compared to high-skill periods.

- ACs occur more frequently across much of the Arctic and tend to be stronger during low-skill periods compared to high-skill periods.

- ACs tend to be embedded in more favorable dynamic and thermodynamic environments for development and intensification during low-skill periods compared to high-skill periods.

Summary

- AC-centered composites for strong low-skill ACs suggest the following:
  - Strong low-skill ACs interact with TPVs in a region of strong lower-to-midtropospheric baroclinicity and relatively large lower-to-midtropospheric Eady growth rates.
  - Strong low-skill ACs are associated with a well-defined corridor of IVT and well-defined regions of latent heating.
  - A combination of TPV–AC interactions, baroclinic processes, and latent heating likely contributes to the development and intensification of strong low-skill ACs.

Summary

- The ESA of AC16 suggests that the predictability of AC16 is sensitive to the amplitude and strength of an upper-tropospheric trough, and to the strength of an embedded TPV, upstream of AC16.

- It is speculated from the ESA of AC16 that a more amplified and stronger upper-tropospheric trough, and a stronger embedded TPV, upstream of AC16 are associated with greater downstream upper-tropospheric flow amplification and greater intensification of AC16.

- It is also speculated from the ESA of AC16 that the position of a region of latent heating associated with AC16 may matter more to the predictability of AC16 than the magnitude of latent heating.

Acknowledgments

- Lance and Dan
- Steven, Andrea, and Ryan
- Faculty and staff
- Friends and fellow graduate students
- Family

Questions?

Extra Slides

Arctic forecast skill

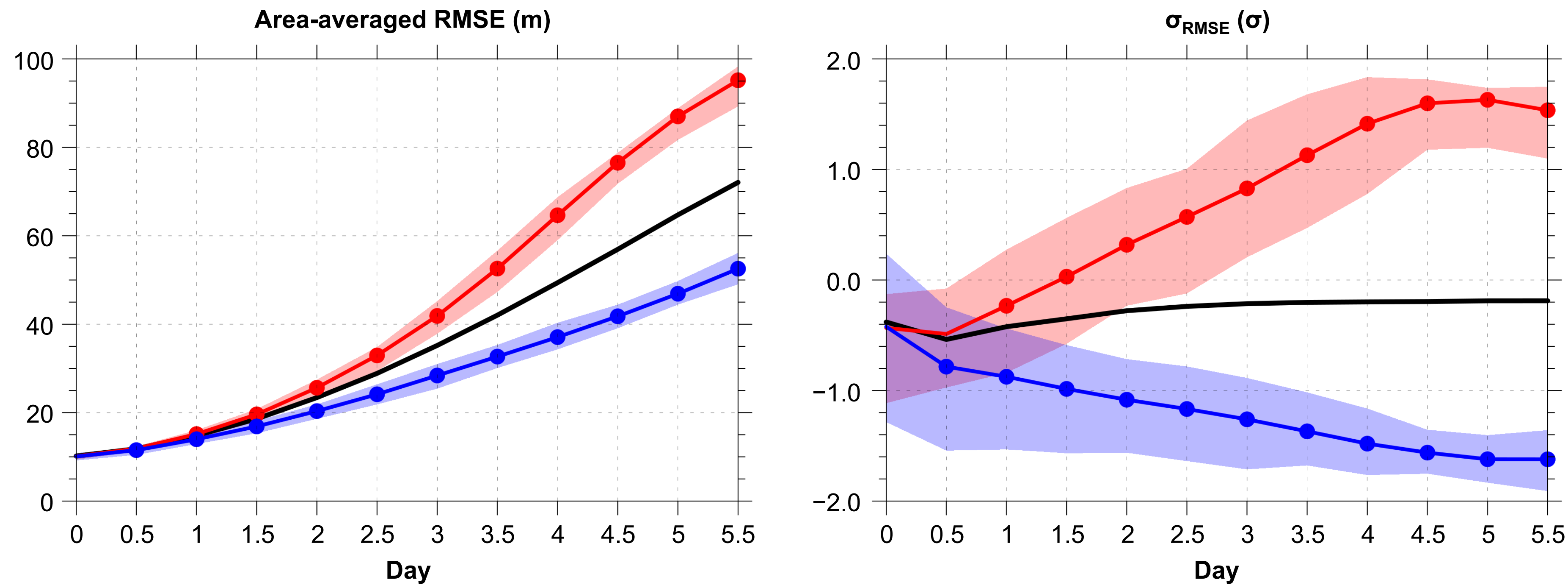

Low-skill mean

High-skill mean

2007–2017 climo mean

Statistically significant difference with respect to climo at 95% confidence level

Shading: Interquartile range

AO index

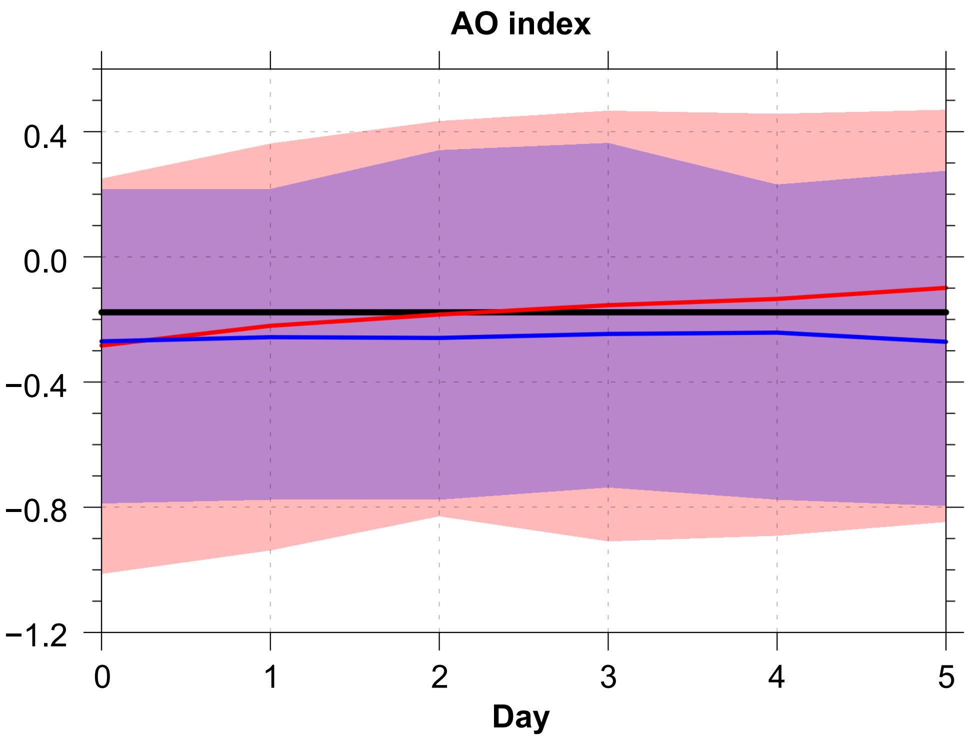

Low-skill mean   High-skill mean   2007–2017 climo mean   **Shading:** Interquartile range

Arctic environment

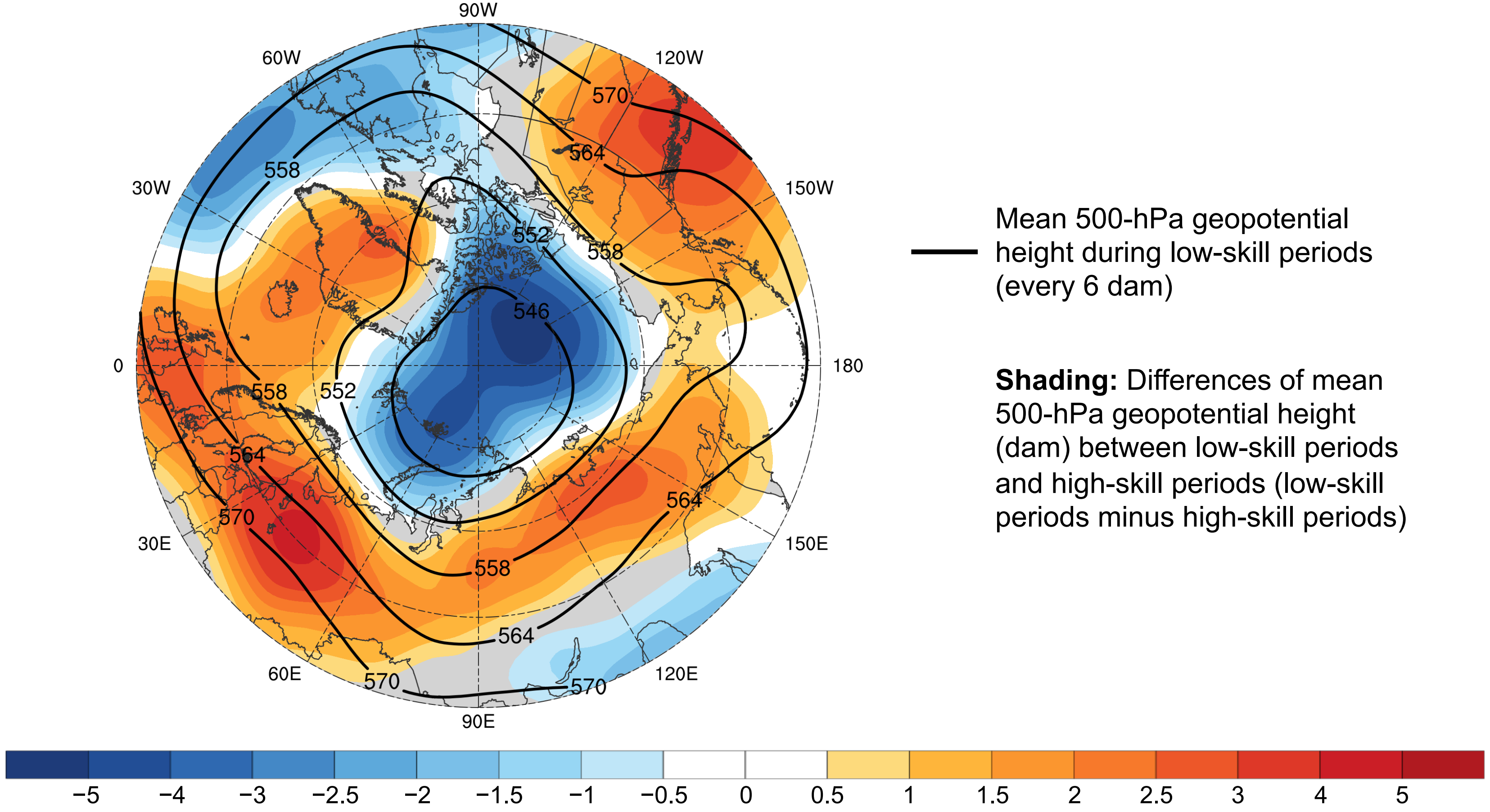

Mean 500-hPa geopotential height during low-skill periods (every 6 dam)

Shading: Differences of mean 500-hPa geopotential height (dam) between low-skill periods and high-skill periods (low-skill periods minus high-skill periods)

Arctic environment

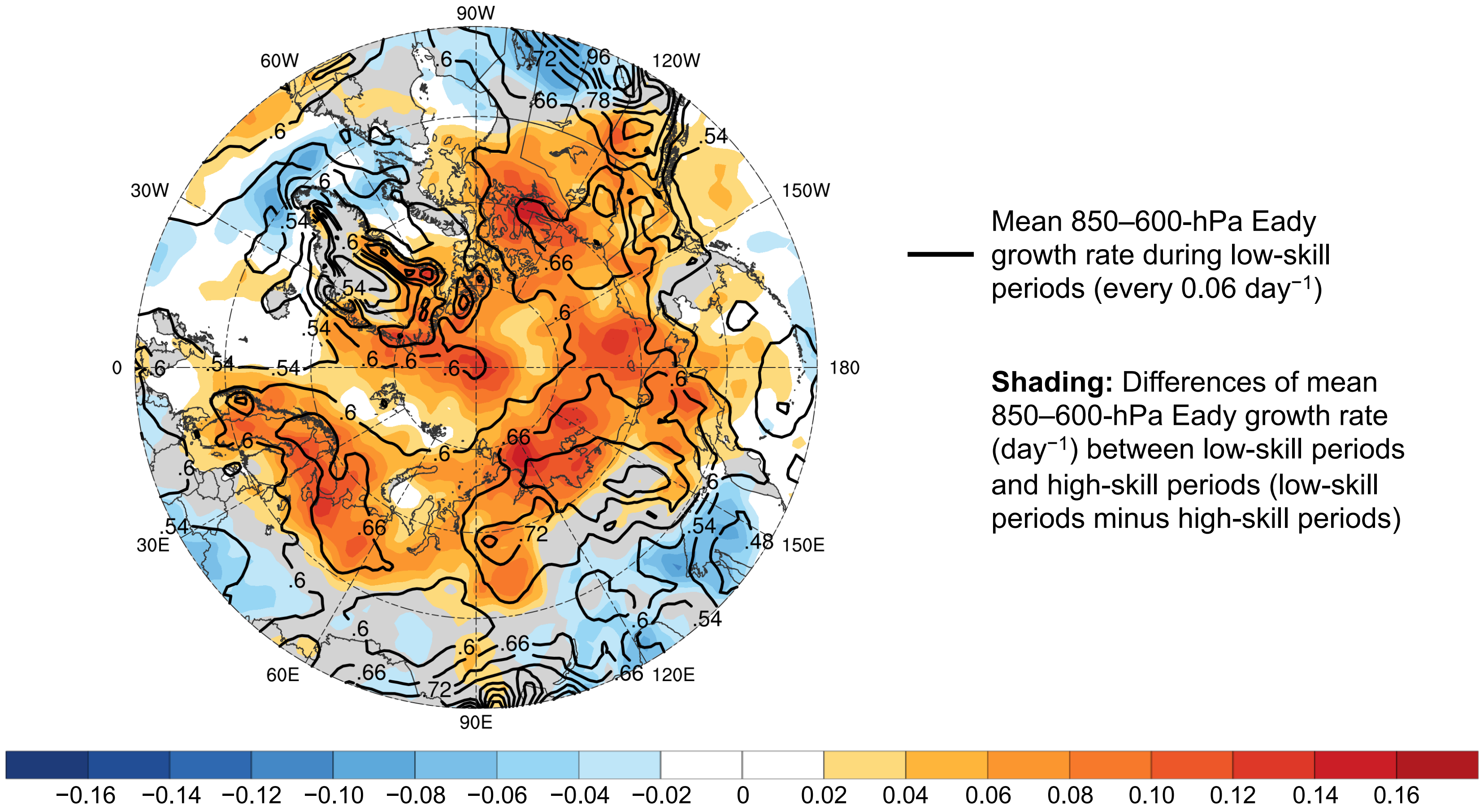

Mean 850–600-hPa Eady growth rate during low-skill periods (every 0.06 day^{-1})

Shading: Differences of mean 850–600-hPa Eady growth rate (day^{-1}) between low-skill periods and high-skill periods (low-skill periods minus high-skill periods)

Arctic environment

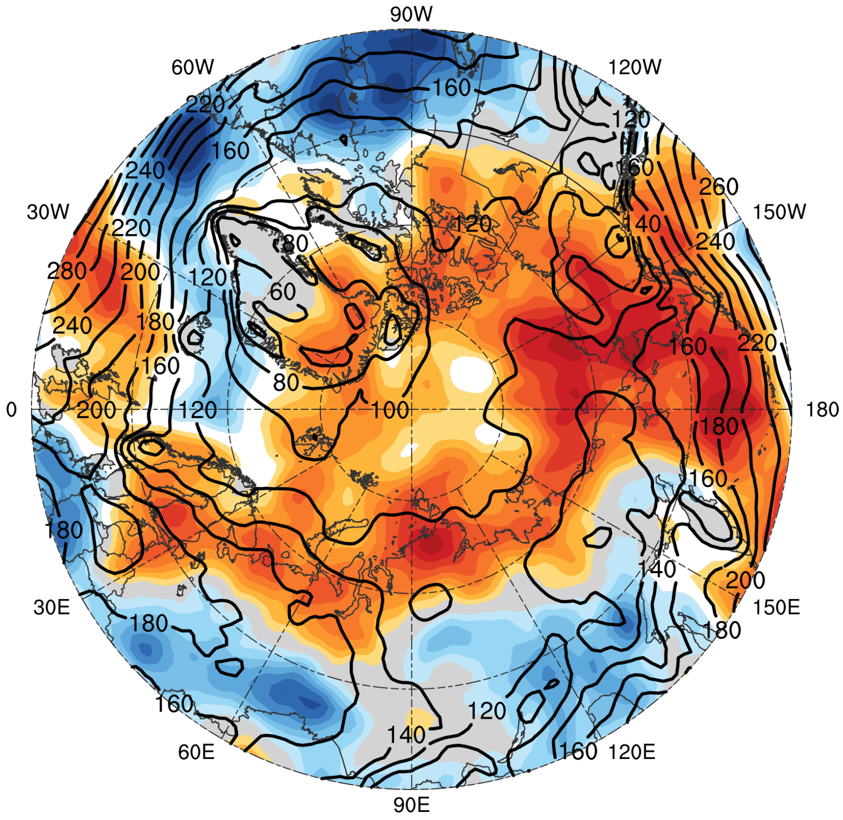

Mean 1000–300-hPa IVT during low-skill periods (every 20 kg m^{-1} s^{-1})

Shading: Differences of mean 1000–300-hPa IVT (kg m^{-1} s^{-1}) between low-skill periods and high-skill periods (low-skill periods minus high-skill periods)

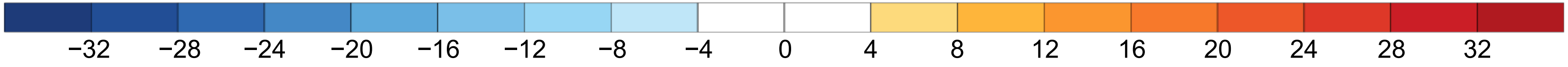

AC characteristics

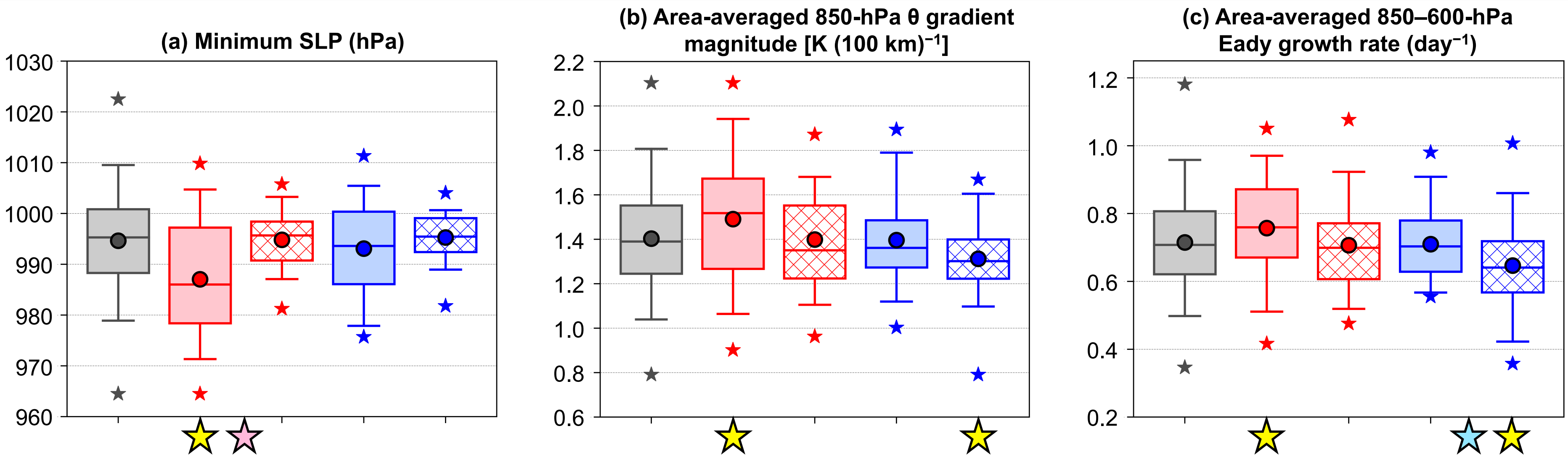

ACs during climatology (*N* = 730)

Low-skill ACs during low-skill periods (*N* = 51)

High-skill ACs during low-skill periods (*N* = 51)

Low-skill ACs during high-skill periods (*N* = 35)

High-skill ACs during high-skill periods (*N* = 35)

Distribution of most extreme value of quantities characterizing ACs when the ACs are located in the Arctic during the various periods.

95%
75%
Median
25%
5%

Mean

Min/ Max

Statistically significant difference with respect to climatology at 95% confidence level

Statistically significant difference between low-skill ACs during low-skill periods and high-skill ACs during low-skill periods at 95% confidence level

Statistically significant difference between low-skill ACs during high-skill periods and high-skill ACs during high-skill periods at 95% confidence level

AC characteristics

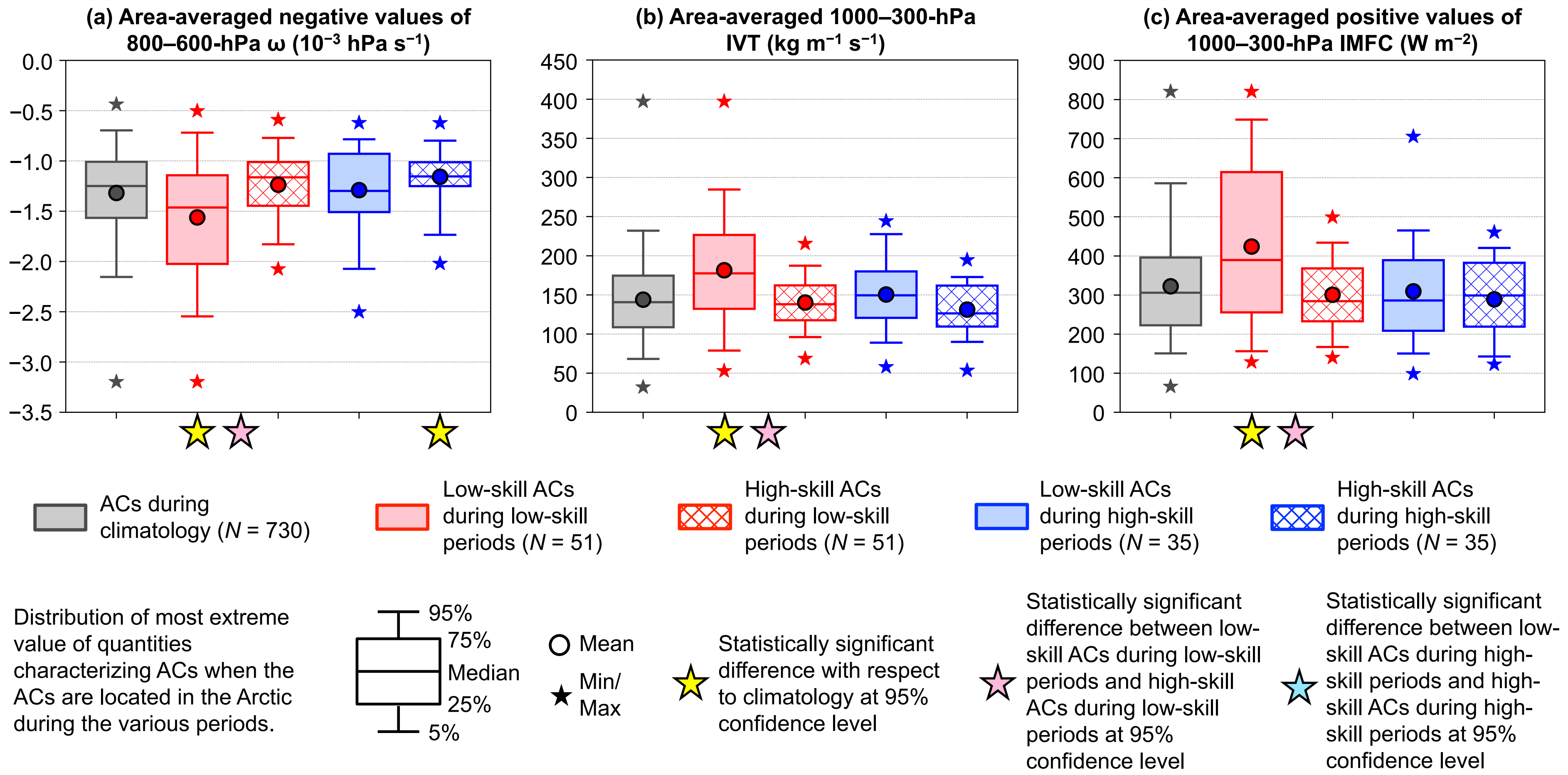

AC track frequency

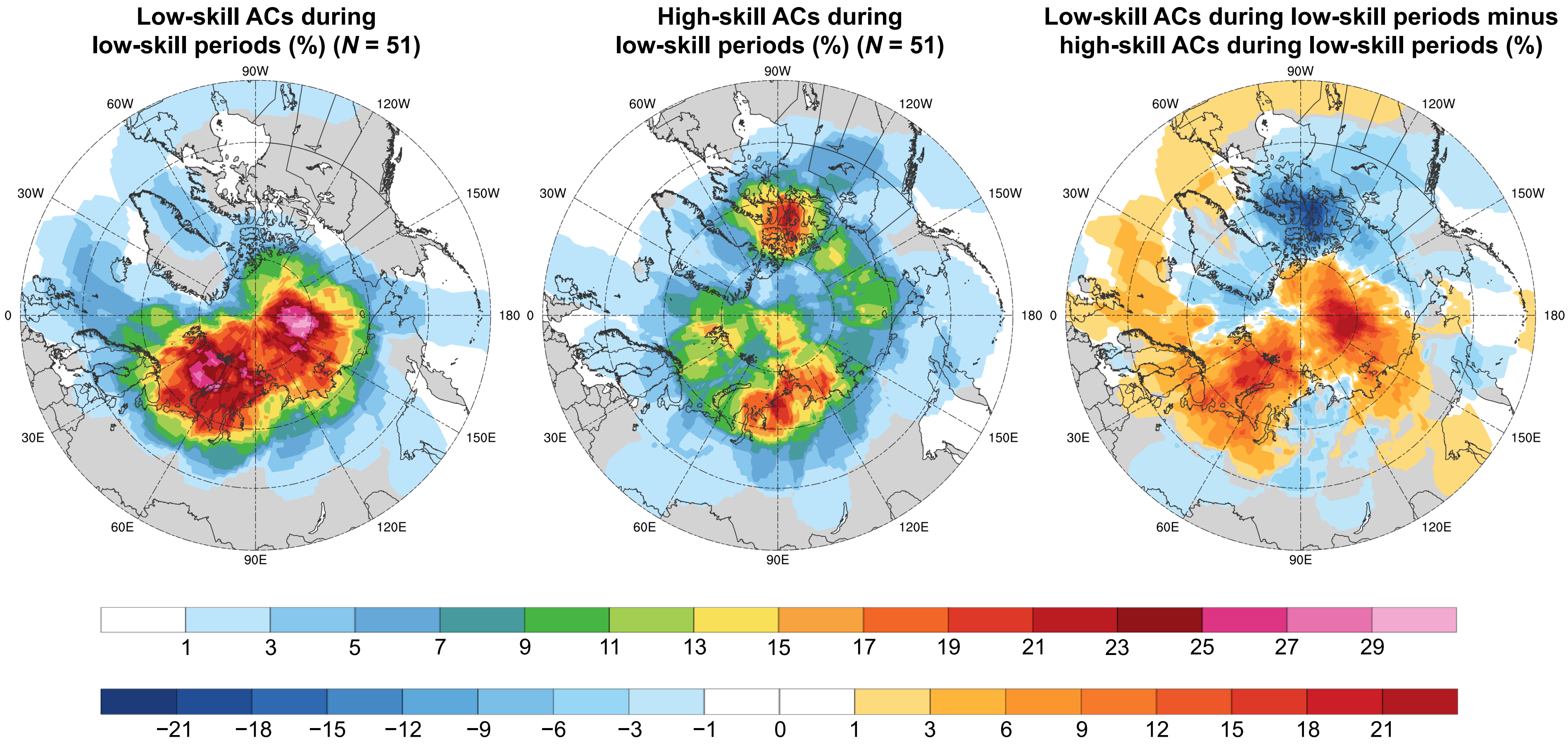

AC track frequency

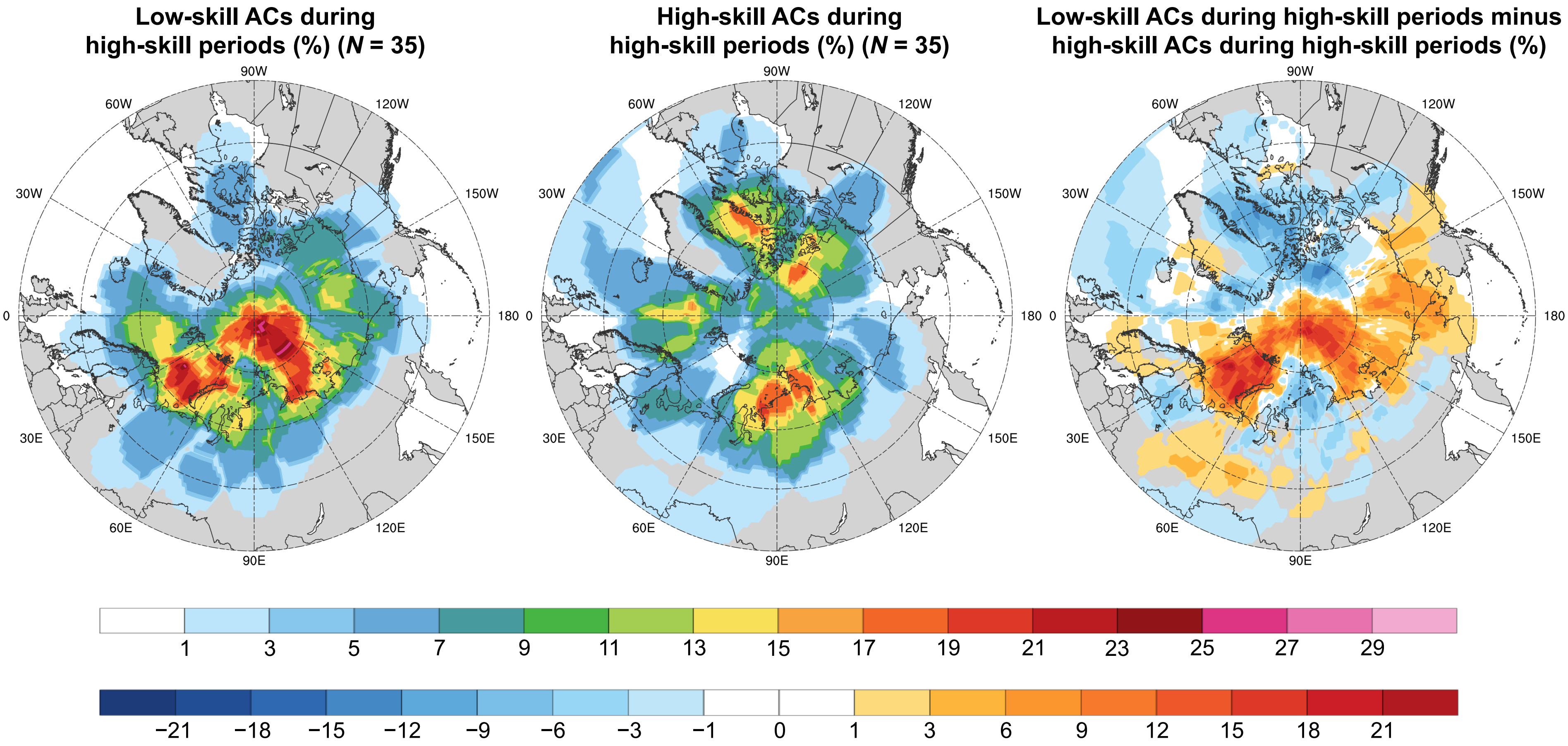

AC-centered composites

- For each lag time:
  - Determine the mean latitude and mean longitude of the ACs.
  - Rotate and project each ERA5 grid onto a 25-km polar Equal-Area Scalable Earth 2.0 (EASE2) grid (Brodzik et al. 2012), such that the AC center is located a 0°E, which corresponds to the y-axis of the EASE2 grid.
  - Shift each EASE2 grid north or south along the y-axis, such that the AC center is located at the grid point closest to the mean latitude of the ACs.
  - Project each shifted EASE2 grid onto a 0.25° latitude–longitude grid and then rotate each grid such that the AC center is located at mean longitude of the ACs.

Strong high-skill ACs

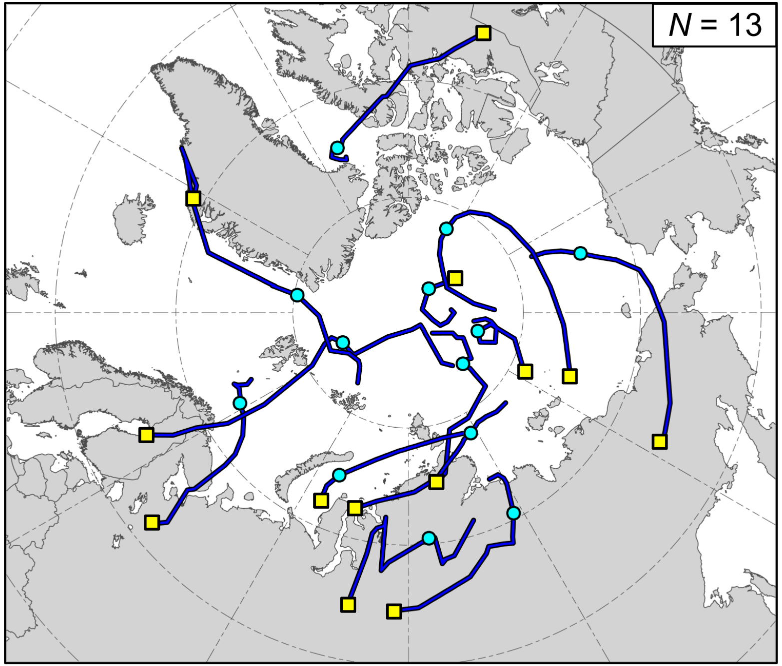

AC location at earliest valid lag hour

AC location at t_{low} (time of lowest SLP of AC when in Arctic)

Blue lines show tracks of ACs during lag hours of –48 to +36 h, every 6 h, relative to t_{low}, when valid

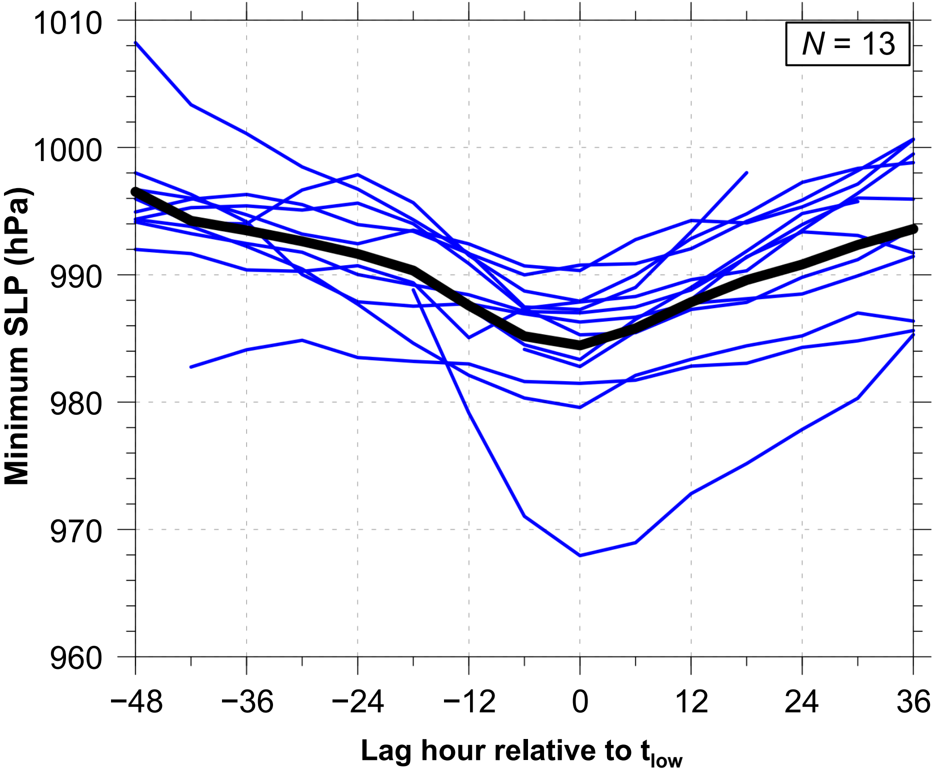

Time series of minimum SLP (hPa) of ACs (blue) and of mean minimum SLP (hPa) of ACs (black) during lag hours of –48 to +36 h, every 6 h, relative to t_{low}, when valid

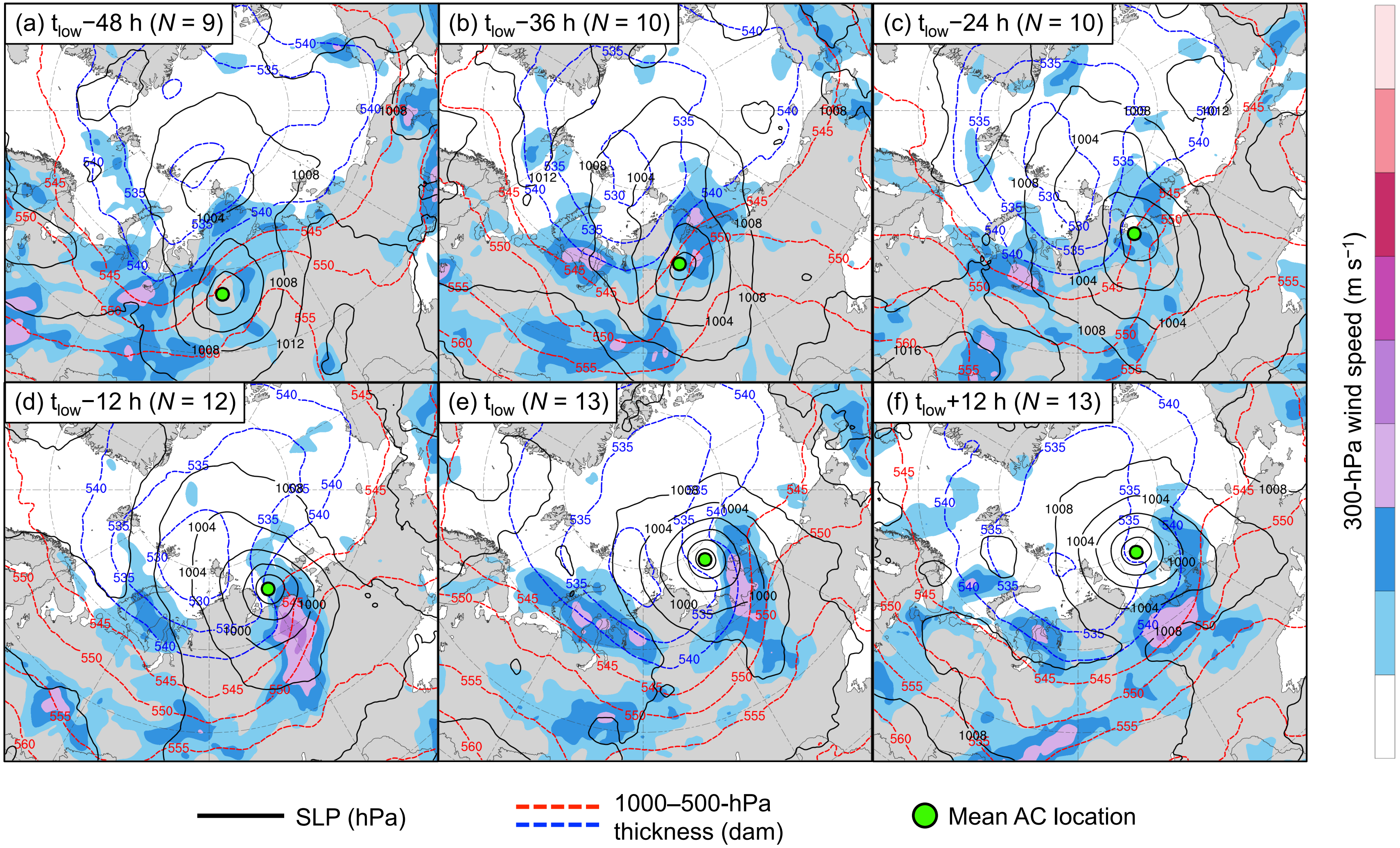

(a) t_low−48 h (N = 9)
(b) t_low−36 h (N = 10)
(c) t_low−24 h (N = 10)
(d) t_low−12 h (N = 12)
(e) t_low (N = 13)
(f) t_low+12 h (N = 13)
300-hPa wind speed (m s−1)
21
24
27
30
33
36
39
42
SLP (hPa)
1000–500-hPa thickness (dam)
Mean AC location

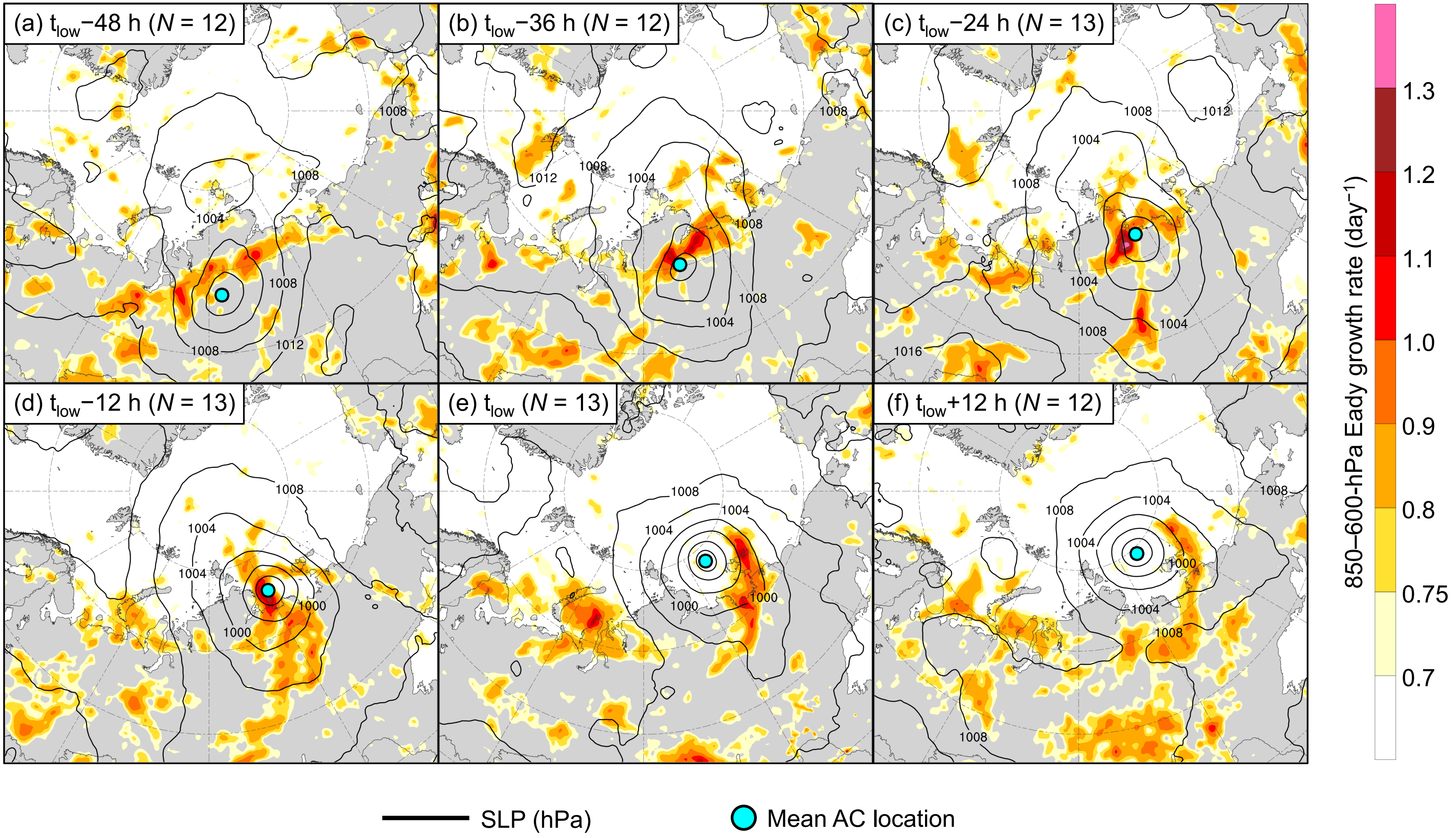

(a) t_{low}−48 h (N = 12)
(b) t_{low}−36 h (N = 12)
(c) t_{low}−24 h (N = 13)
(d) t_{low}−12 h (N = 13)
(e) t_{low} (N = 13)
(f) t_{low}+12 h (N = 12)
850–600-hPa Eady growth rate (day^{-1})
1.3
1.2
1.1
1.0
0.9
0.8
0.75
0.7
SLP (hPa)
Mean AC location

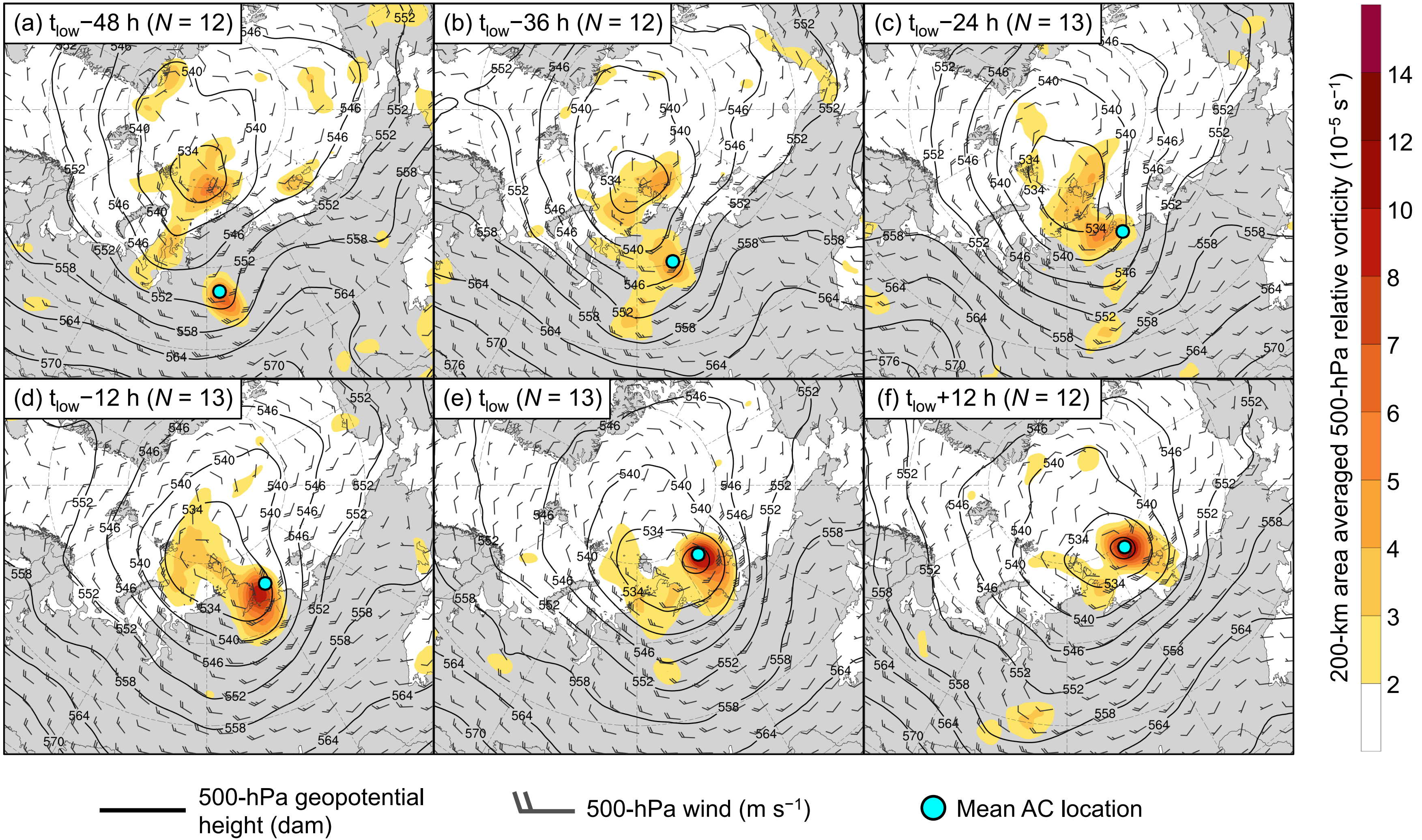

(a) t_{low}−48 h (N = 12)
(b) t_{low}−36 h (N = 12)
(c) t_{low}−24 h (N = 13)
(d) t_{low}−12 h (N = 13)
(e) t_{low} (N = 13)
(f) t_{low}+12 h (N = 12)
200-km area averaged 500-hPa relative vorticity (10^{-5} s^{-1})
2
3
4
5
6
7
8
10
12
14
500-hPa geopotential height (dam)
500-hPa wind (m s^{-1})
Mean AC location

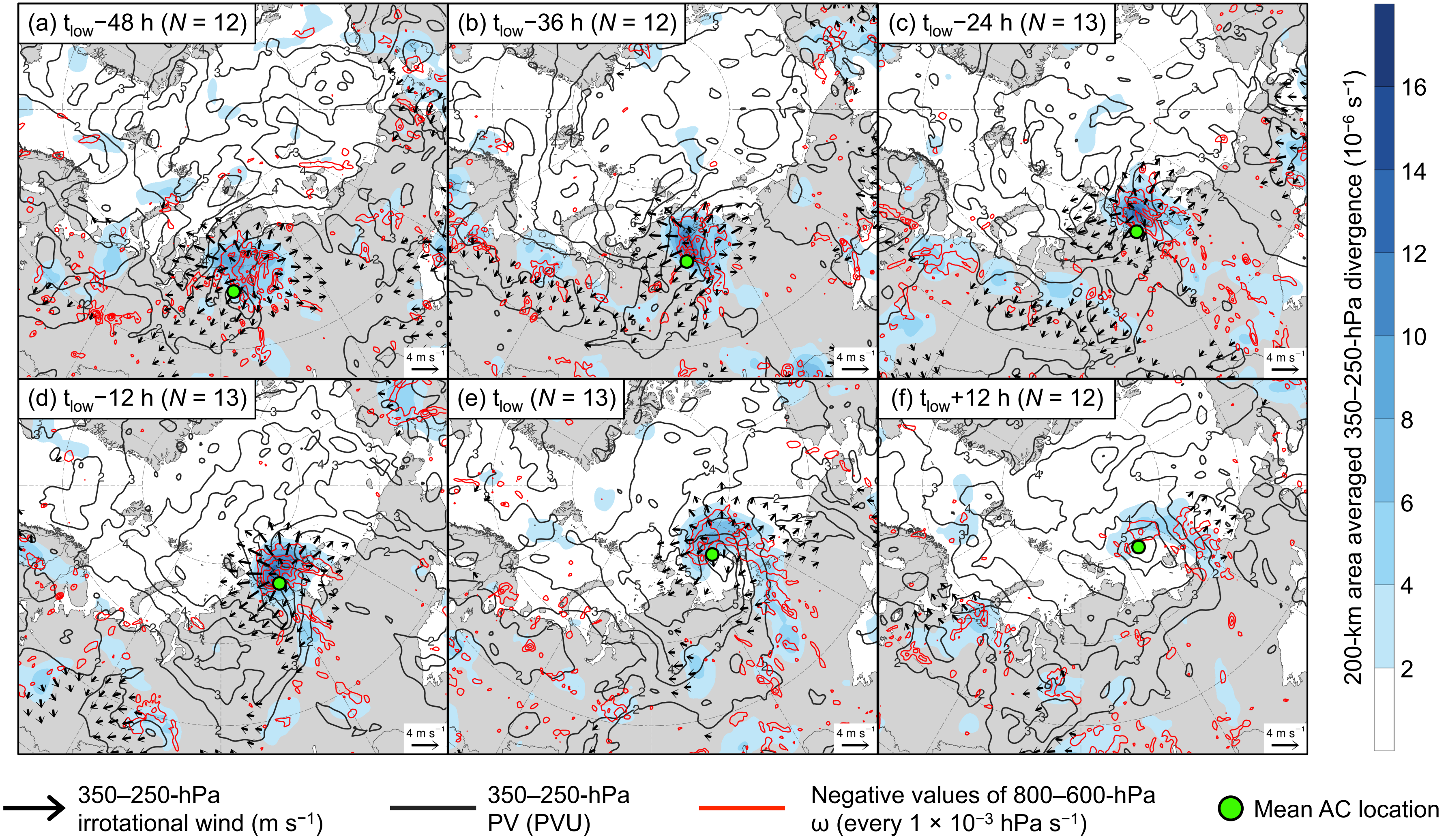

(a) t_low−48 h (N = 12)
(b) t_low−36 h (N = 12)
(c) t_low−24 h (N = 13)
(d) t_low−12 h (N = 13)
(e) t_low (N = 13)
(f) t_low+12 h (N = 12)
4 m s⁻¹
200-km area averaged 350–250-hPa divergence (10⁻⁶ s⁻¹)
2
4
6
8
10
12
14
16
350–250-hPa irrotational wind (m s⁻¹)
350–250-hPa PV (PVU)
Negative values of 800–600-hPa ω (every 1 × 10⁻³ hPa s⁻¹)
Mean AC location

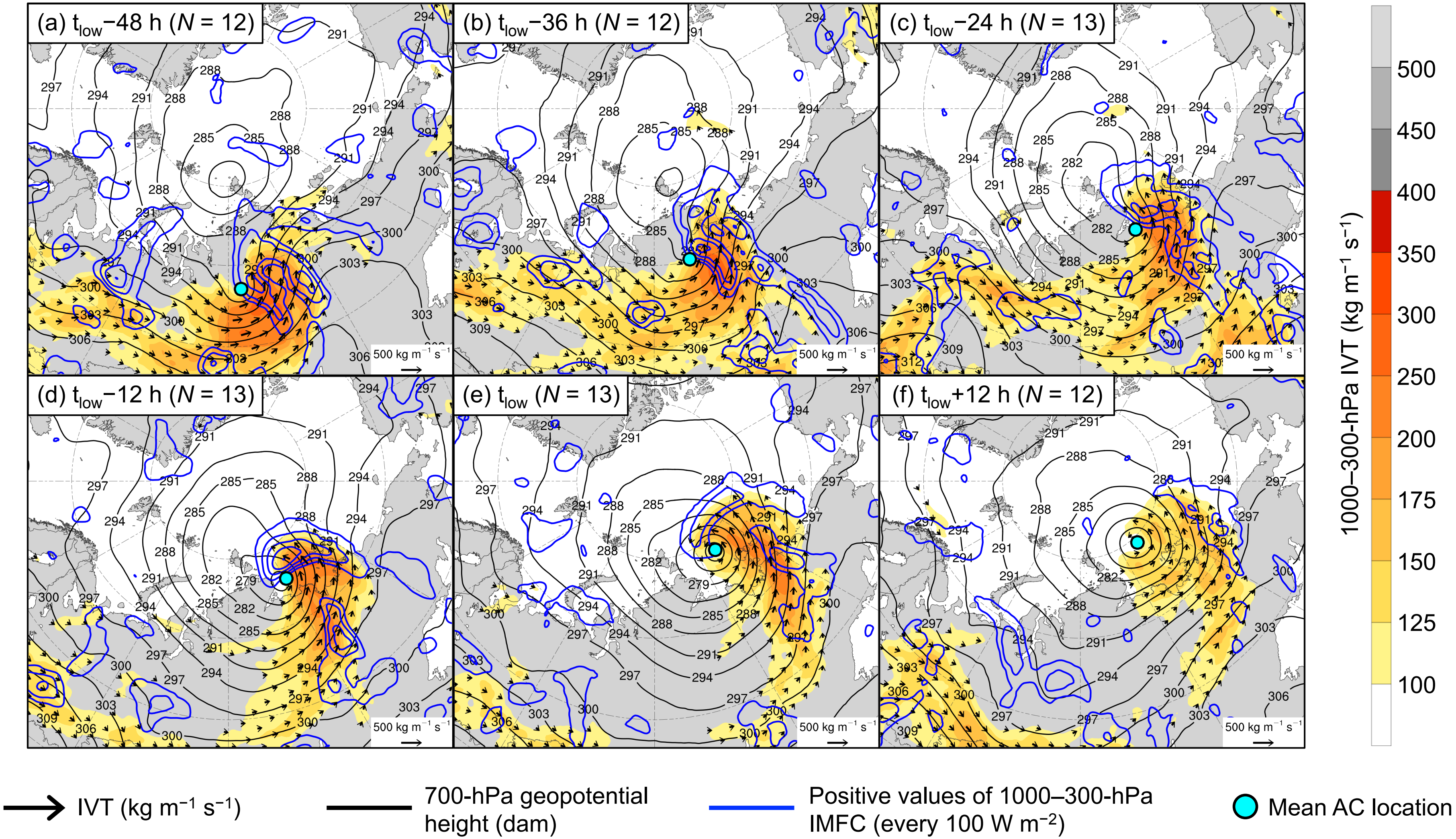

(a) t_{low}−48 h (N = 12)
(b) t_{low}−36 h (N = 12)
(c) t_{low}−24 h (N = 13)
(d) t_{low}−12 h (N = 13)
(e) t_{low} (N = 13)
(f) t_{low}+12 h (N = 12)
500 kg m⁻¹ s⁻¹
1000–300-hPa IVT (kg m⁻¹ s⁻¹)
100 125 150 175 200 250 300 350 400 450 500
IVT (kg m⁻¹ s⁻¹)
700-hPa geopotential height (dam)
Positive values of 1000–300-hPa IMFC (every 100 W m⁻²)
Mean AC location

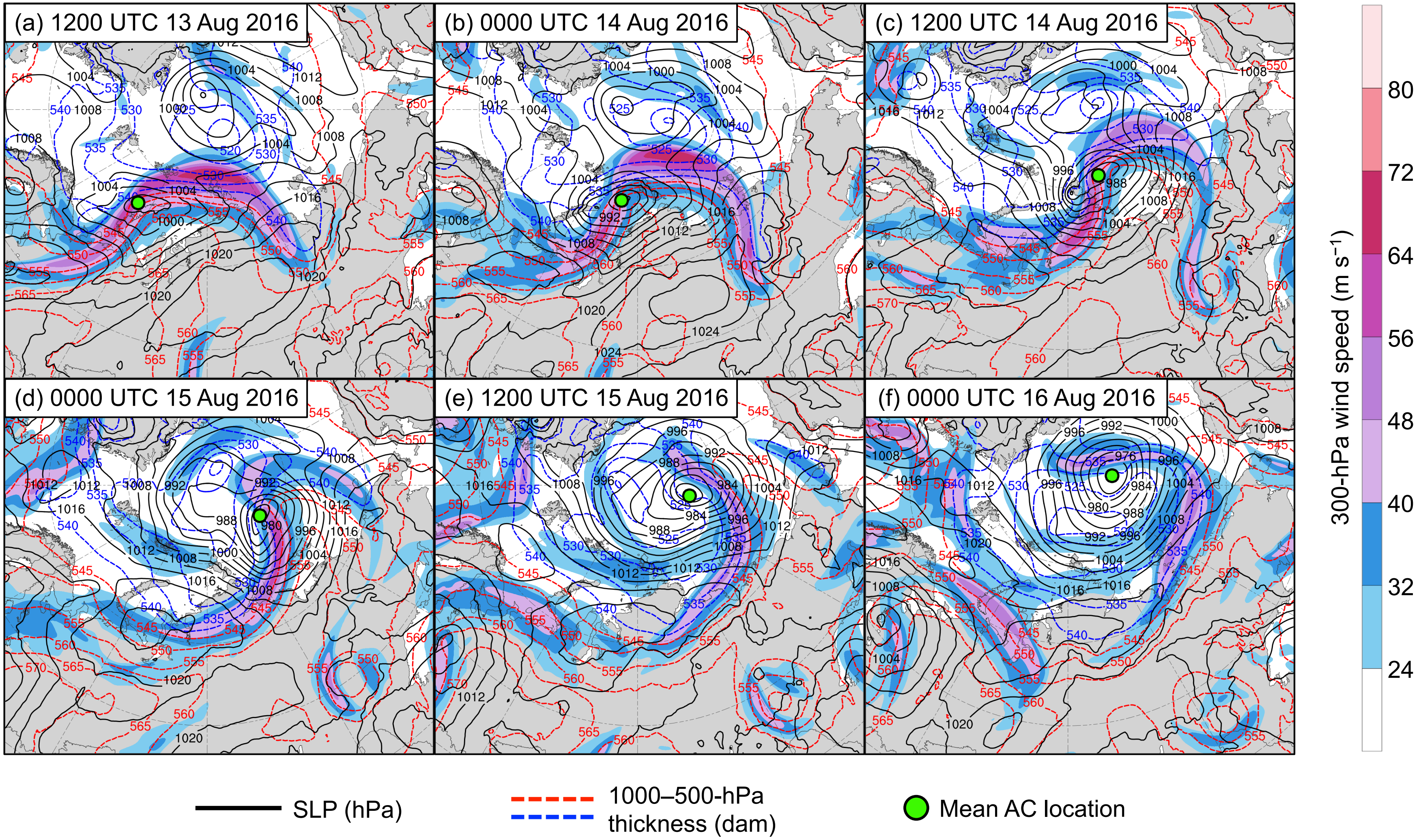

(a) 1200 UTC 13 Aug 2016
(b) 0000 UTC 14 Aug 2016
(c) 1200 UTC 14 Aug 2016
(d) 0000 UTC 15 Aug 2016
(e) 1200 UTC 15 Aug 2016
(f) 0000 UTC 16 Aug 2016
300-hPa wind speed (m s−1)
80
72
64
56
48
40
32
24
SLP (hPa)
1000–500-hPa thickness (dam)
Mean AC location

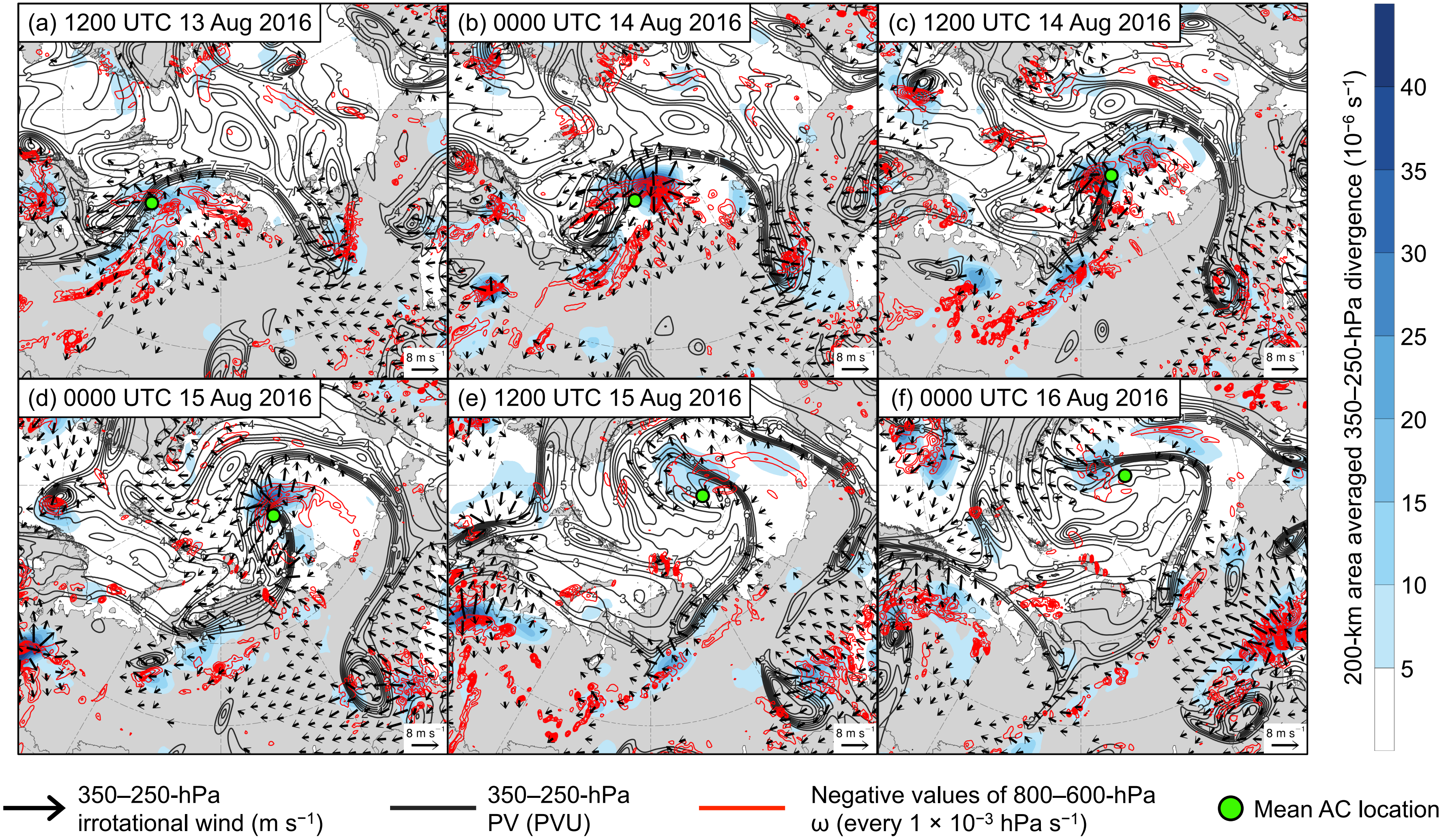
(a) 1200 UTC 13 Aug 2016
(b) 0000 UTC 14 Aug 2016
(c) 1200 UTC 14 Aug 2016
(d) 0000 UTC 15 Aug 2016
(e) 1200 UTC 15 Aug 2016
(f) 0000 UTC 16 Aug 2016
8 m s−1
200-km area averaged 350–250-hPa divergence (10−6 s−1)
5
10
15
20
25
30
35
40
350–250-hPa irrotational wind (m s−1)
350–250-hPa PV (PVU)
Negative values of 800–600-hPa ω (every 1 × 10−3 hPa s−1)
Mean AC location

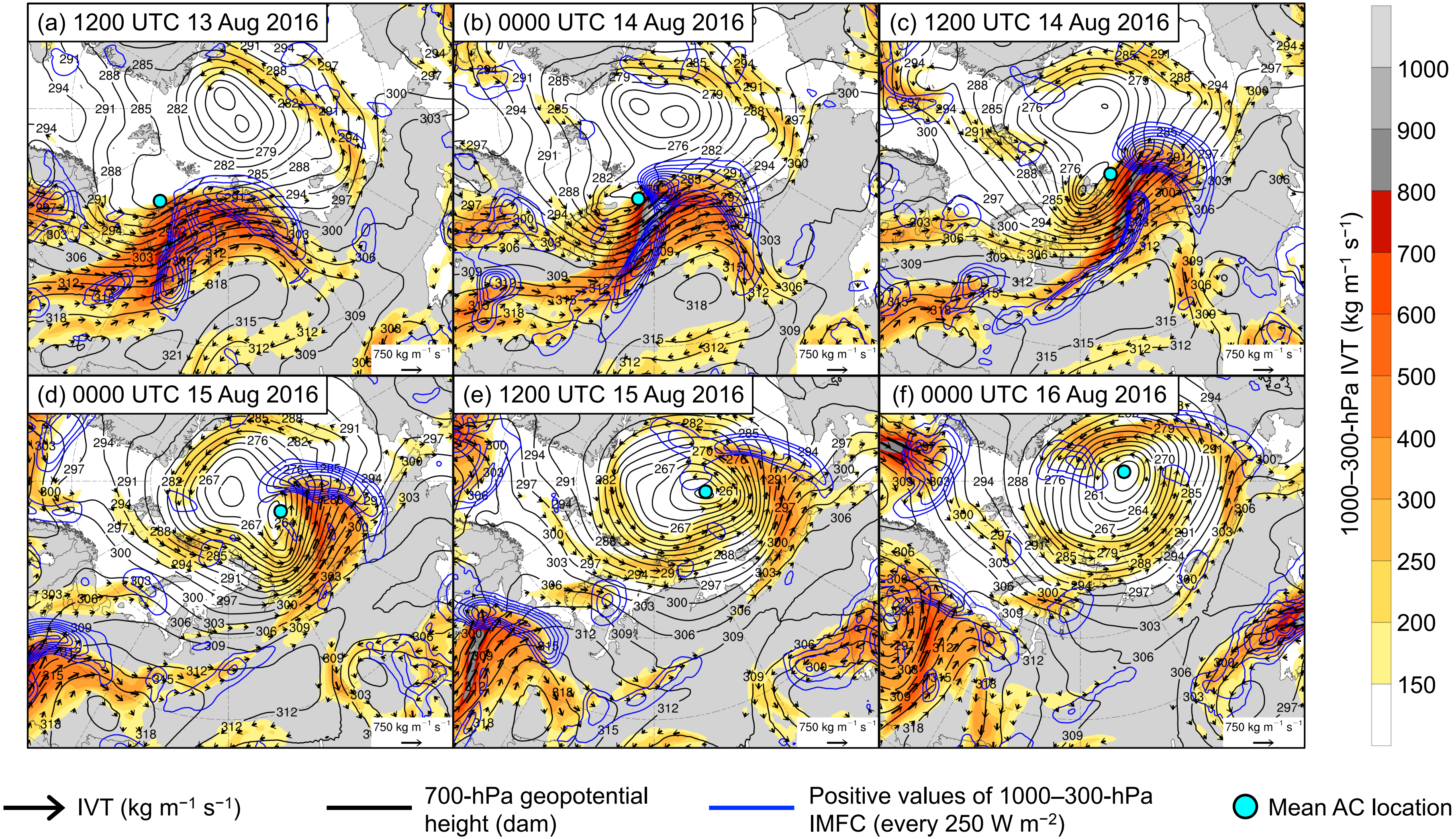

(a) 1200 UTC 13 Aug 2016
(b) 0000 UTC 14 Aug 2016
(c) 1200 UTC 14 Aug 2016
(d) 0000 UTC 15 Aug 2016
(e) 1200 UTC 15 Aug 2016
(f) 0000 UTC 16 Aug 2016
750 kg m⁻¹ s⁻¹
1000–300-hPa IVT (kg m⁻¹ s⁻¹)
1000
900
800
700
600
500
400
300
250
200
150
IVT (kg m⁻¹ s⁻¹)
700-hPa geopotential height (dam)
Positive values of 1000–300-hPa IMFC (every 250 W m⁻²)
Mean AC location

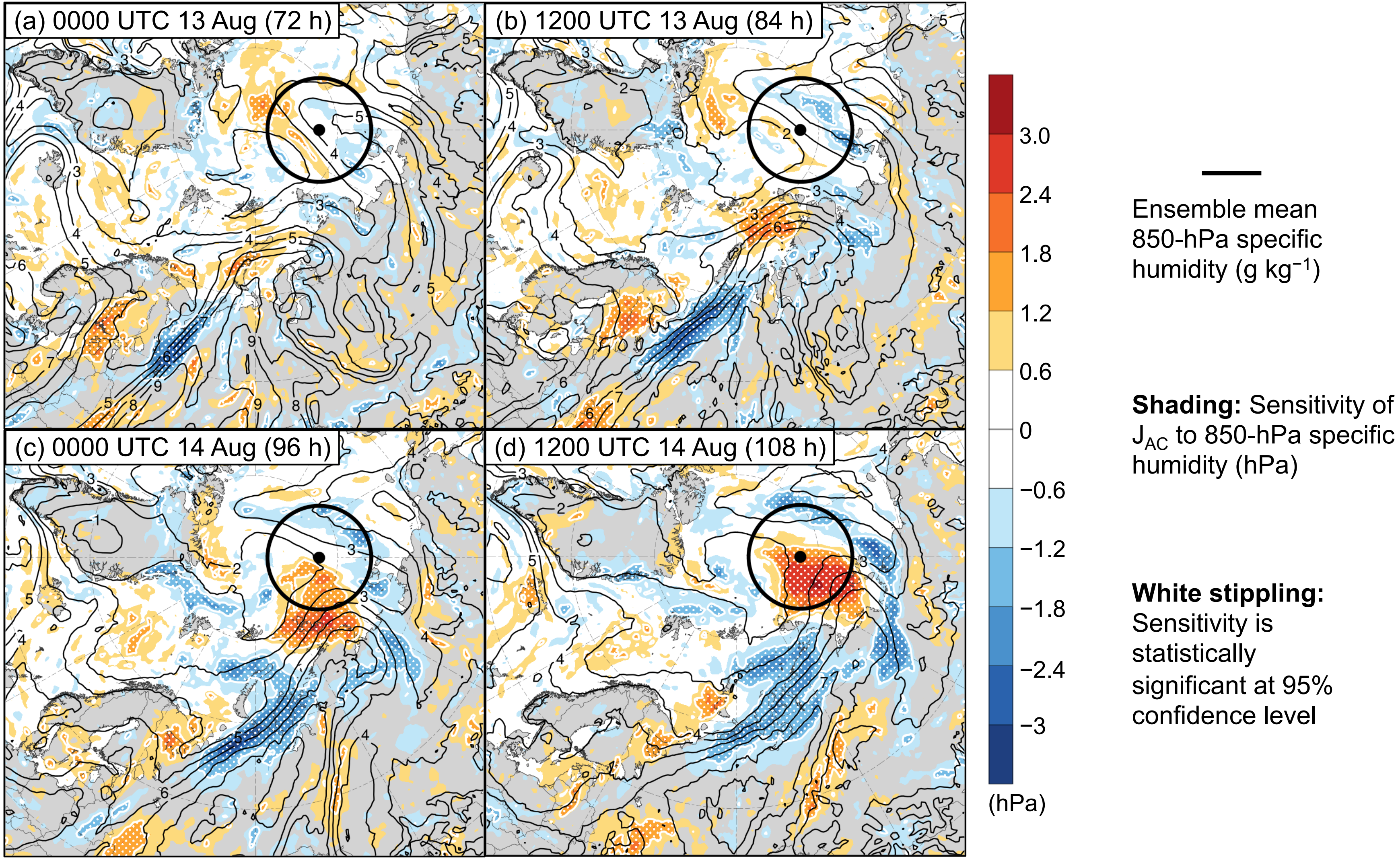
(a) 0000 UTC 13 Aug (72 h)
(b) 1200 UTC 13 Aug (84 h)
(c) 0000 UTC 14 Aug (96 h)
(d) 1200 UTC 14 Aug (108 h)
3.0
2.4
1.8
1.2
0.6
0
−0.6
−1.2
−1.8
−2.4
−3
(hPa)
Ensemble mean 850-hPa specific humidity (g kg^{-1})
Shading: Sensitivity of J_{AC} to 850-hPa specific humidity (hPa)
White stippling: Sensitivity is statistically significant at 95% confidence level

Data and methods

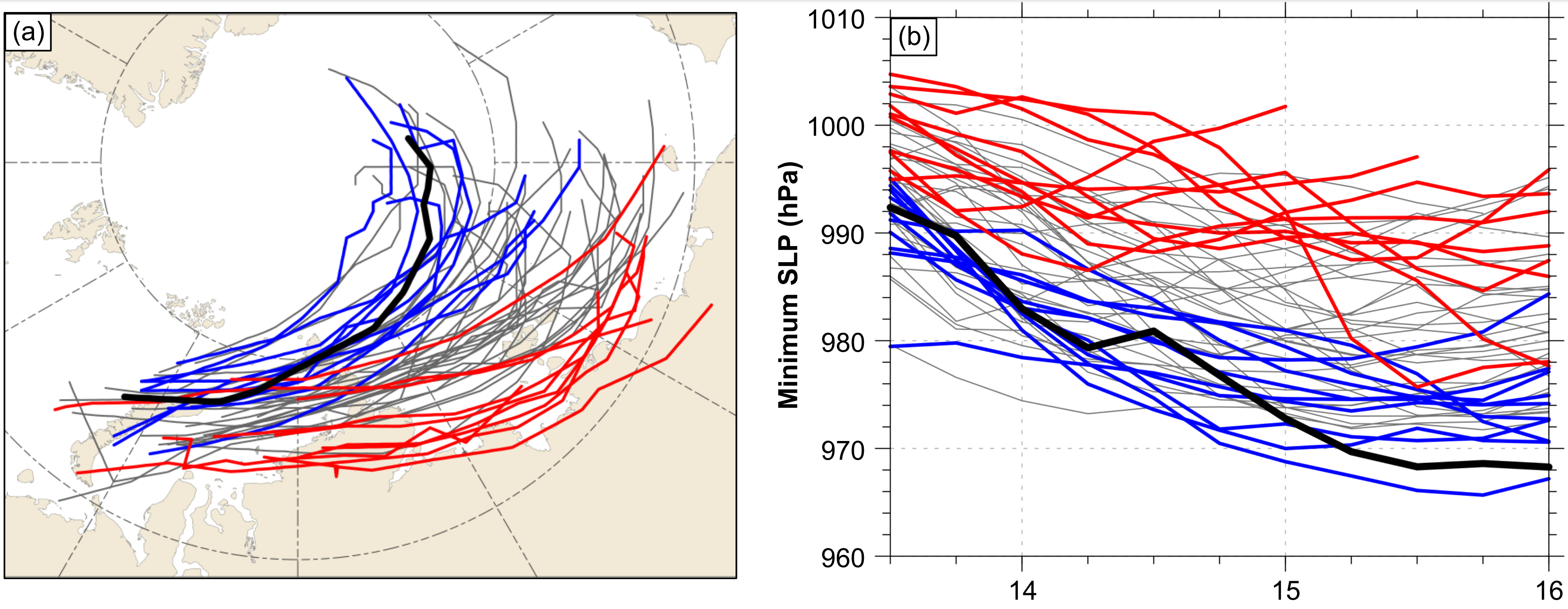

(a) Track and (b) intensity during 1200 UTC 13–0000 UTC 16 Aug 2016

ERA5

Most-accurate ensemble members (N = 10)

Least-accurate ensemble members (N = 10)

All other ensemble members (N = 31)

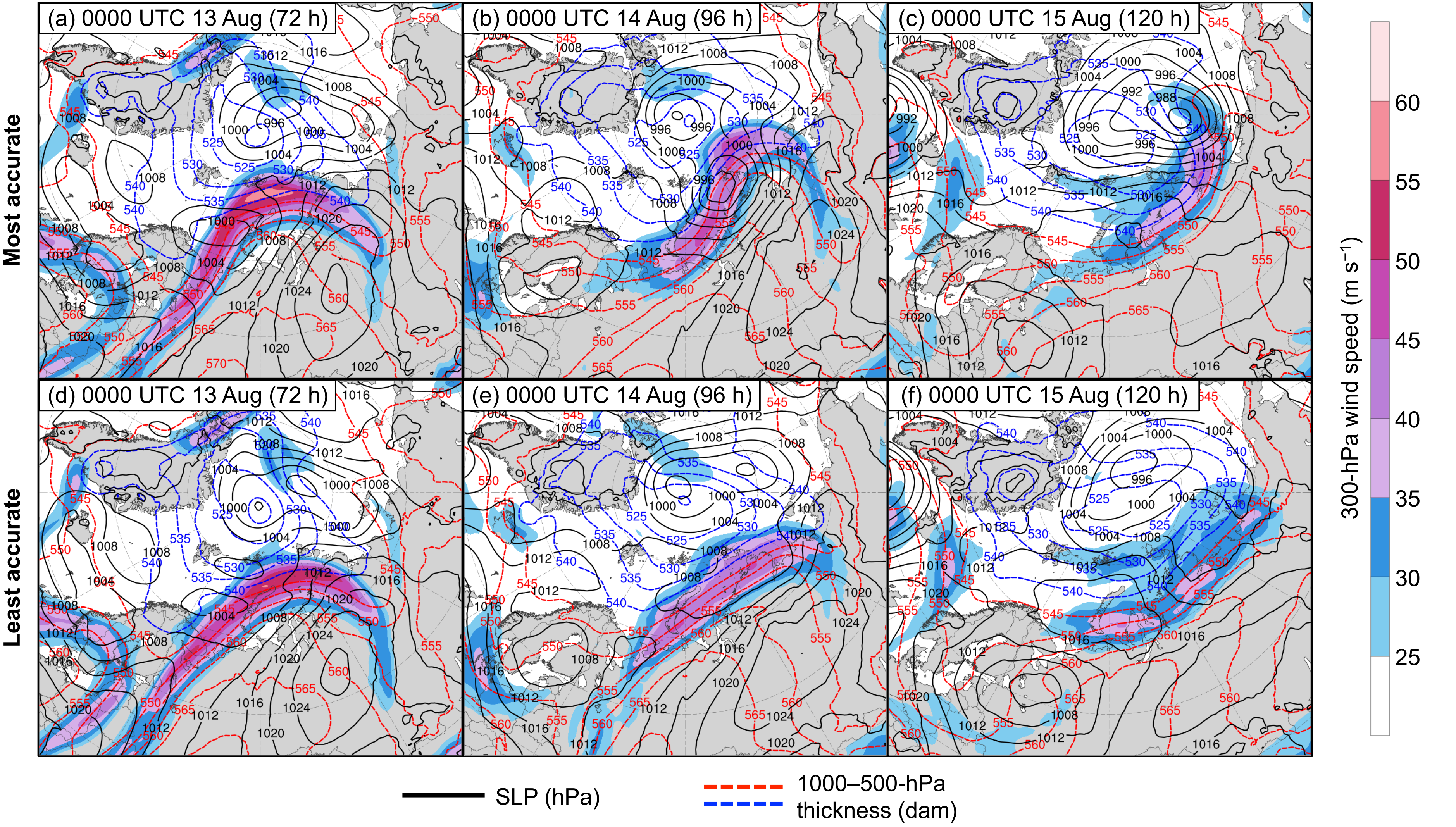
(a) 0000 UTC 13 Aug (72 h)
(b) 0000 UTC 14 Aug (96 h)
(c) 0000 UTC 15 Aug (120 h)
(d) 0000 UTC 13 Aug (72 h)
(e) 0000 UTC 14 Aug (96 h)
(f) 0000 UTC 15 Aug (120 h)
Most accurate
Least accurate
300-hPa wind speed (m s^{-1})
25
30
35
40
45
50
55
60
SLP (hPa)
1000–500-hPa thickness (dam)

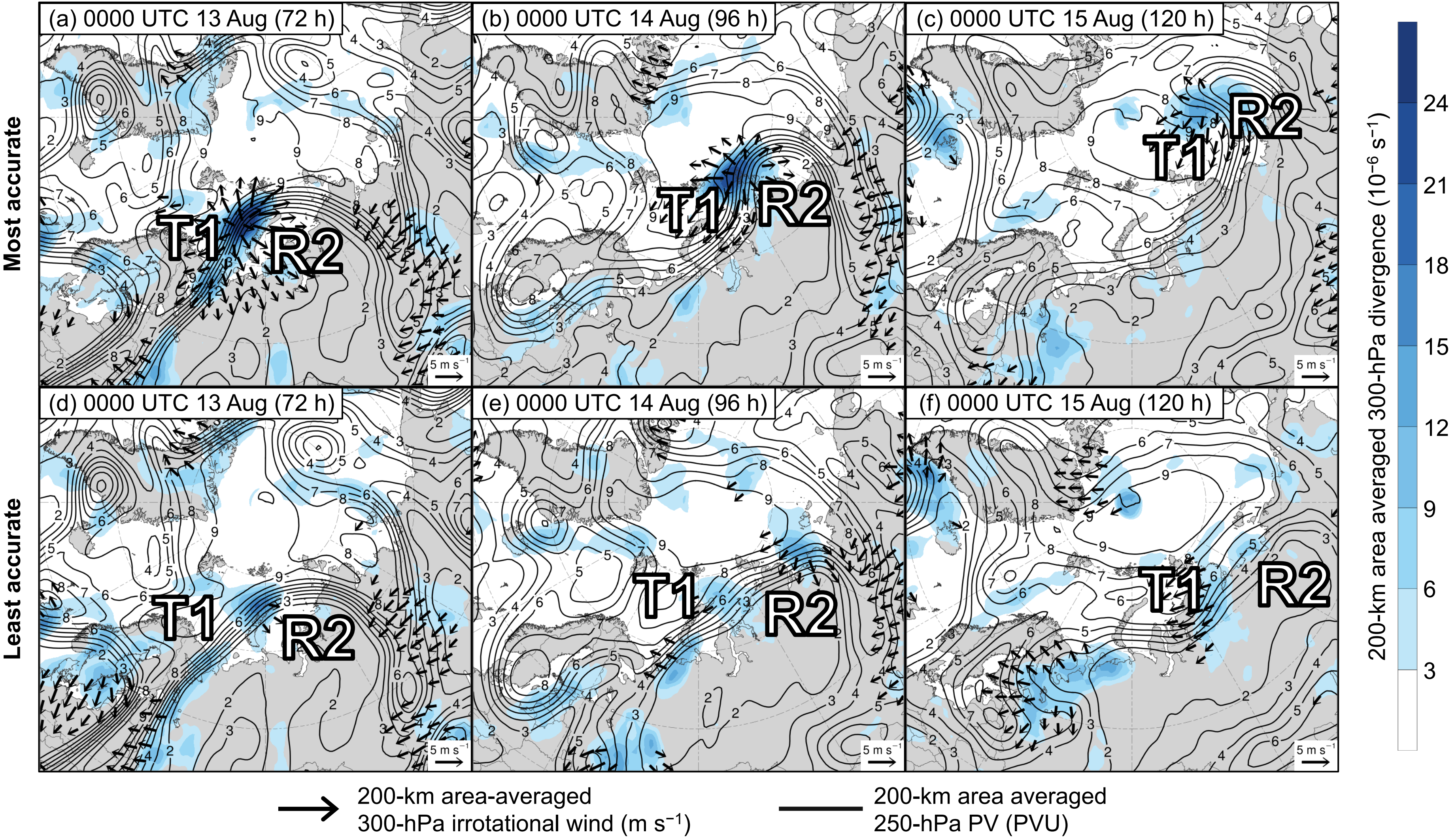

(a) 0000 UTC 13 Aug (72 h)
(b) 0000 UTC 14 Aug (96 h)
(c) 0000 UTC 15 Aug (120 h)
(d) 0000 UTC 13 Aug (72 h)
(e) 0000 UTC 14 Aug (96 h)
(f) 0000 UTC 15 Aug (120 h)
Most accurate
Least accurate
T1
R2
5 m s⁻¹
200-km area averaged 300-hPa divergence (10⁻⁶ s⁻¹)
3
6
9
12
15
18
21
24
200-km area-averaged 300-hPa irrotational wind (m s⁻¹)
200-km area averaged 250-hPa PV (PVU)

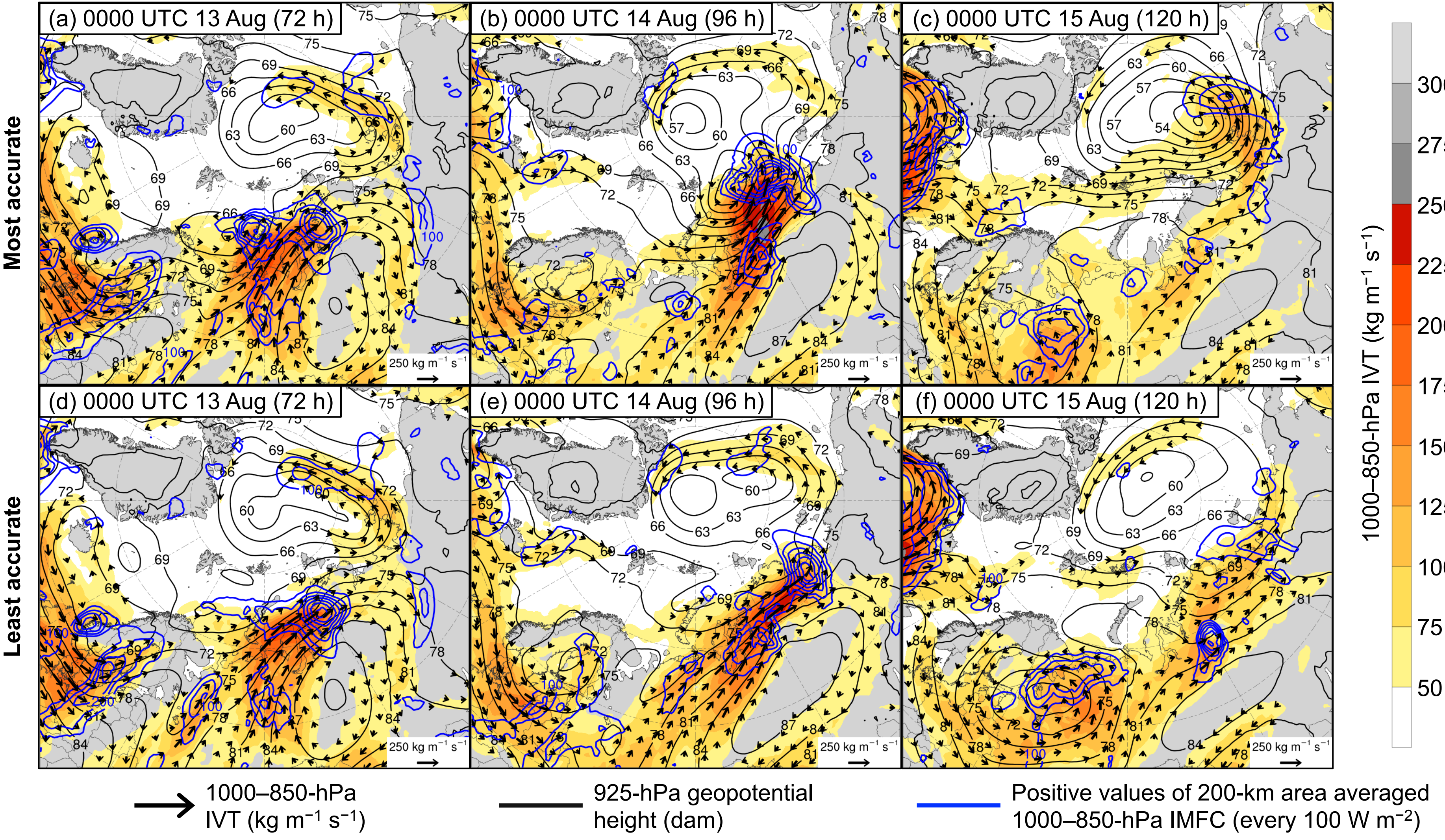

(a) 0000 UTC 13 Aug (72 h)
(b) 0000 UTC 14 Aug (96 h)
(c) 0000 UTC 15 Aug (120 h)
(d) 0000 UTC 13 Aug (72 h)
(e) 0000 UTC 14 Aug (96 h)
(f) 0000 UTC 15 Aug (120 h)
Most accurate
Least accurate
250 kg m^{-1} s^{-1}
1000–850-hPa IVT (kg m^{-1} s^{-1})
50
75
100
125
150
175
200
225
250
275
300
1000–850-hPa IVT (kg m^{-1} s^{-1})
925-hPa geopotential height (dam)
Positive values of 200-km area averaged 1000–850-hPa IMFC (every 100 W m^{-2})

Area-averaged quantities at 0000 UTC 14 Aug (96 h)

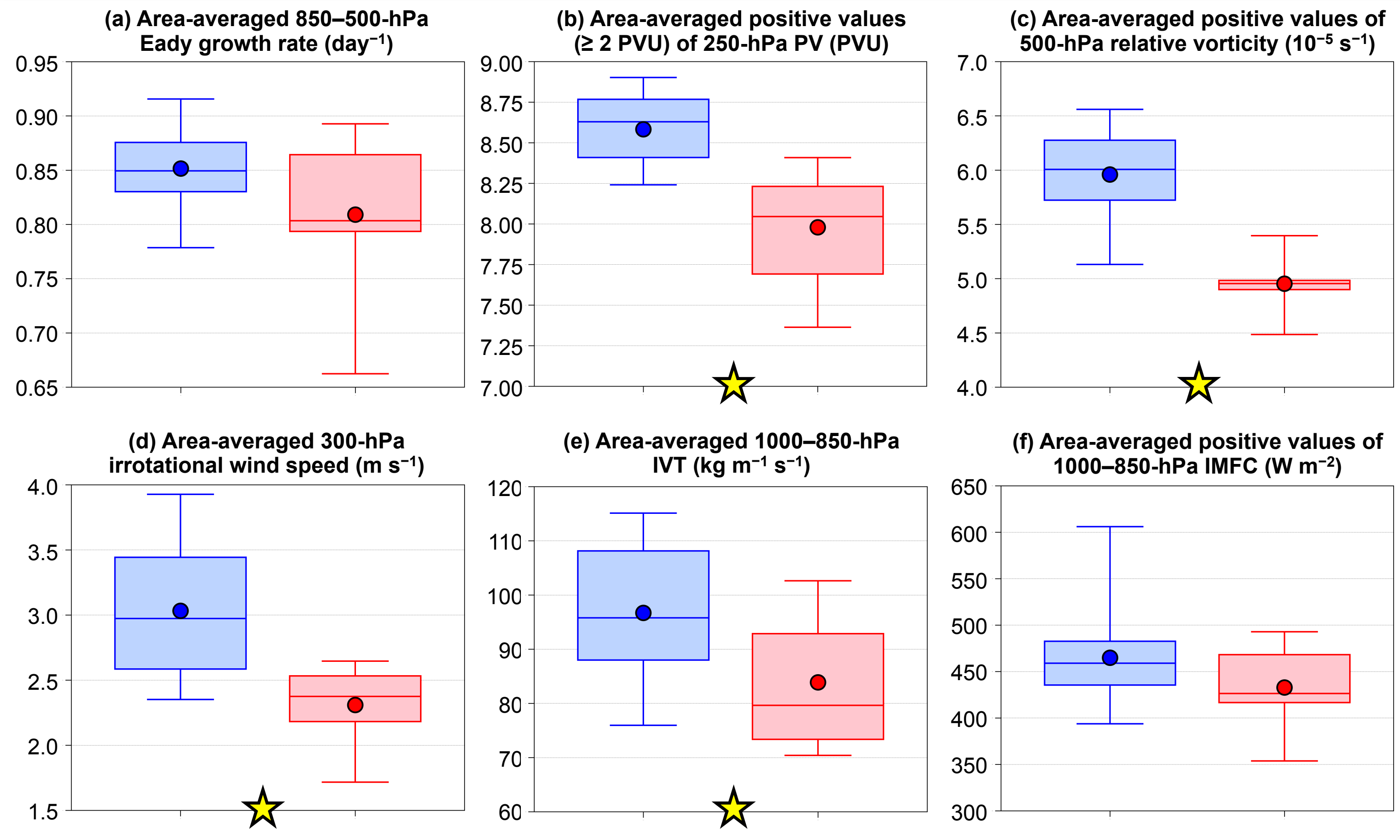

Legend

Distribution of selected quantities area-averaged within a 1000-km radius from center of AC16 at 0000 UTC 14 Aug (96 h)

Blue: Most-accurate ensemble members (N = 10)

Red: Least-accurate ensemble members (N = 10)